Acoustic shielding and interaction effects for strongly heated supersonic twin jets

Pierre Pineau, Christophe Bogey

Acoustic shielding and interaction effects for strongly heated supersonic twin jets

P. Pineau[1, a)] and C. Bogey[1]

Univ Lyon, École Centrale de Lyon, INSA Lyon, Université Claude Bernard Lyon I, CNRS,

Laboratoire de Mécanique des Fluides et d'Acoustique, UMR 5509, F-69134, Ecully, France

(Dated: 22 June 2021)

The effects of jet interactions and acoustic shielding on the noise of strongly heated supersonic twin jets are studied using large-eddy simulations. For that purpose, one single jet and three twin jets separated by distances of 2, 2.4 and 2.8 jet diameters are considered at a Mach number of 3.1 and a stagnation temperature of 2,000 K. The twin jets interact and merge near the end of their potential cores at a position which is shifted downstream when the nozzle spacing increases. For a larger nozzle spacing, the turbulence rates in the plane containing the jets are higher whereas those in the jet midplane are lower. In the near pressure field, the overall acoustic power radiated by the twin jets is lower than that for two non-interacting single jets, which indicates that some of the sound sources are weakened by the jet interactions. A maximum noise reduction of 2 dB is reached in the jet plane, where the acoustic waves produced by one jet are shielded by the other one. Despite the overall noise reduction, some noise components are stronger for the twin jets, suggesting that they generate additional interaction noise. This is the case for the broadband shock-associated noise component and for the noise radiated at low polar angles in the jet midplane. The intensity of interaction noise increases with the nozzle spacing and varies with the turbulence rates in the inner shear layers at the axial position where the twin jets interact.

[a)]Electronic mail: pierre.pineau@ec-lyon.fr

I. INTRODUCTION

The first propulsion stage of rocket launchers usually combines two or more rocket engines ejecting high temperature gases at very high speeds. During lift-off, these supersonic jets radiate intense acoustic waves which are reflected by the ground and propagate upwards, imposing intense transient stresses on the payload fairing. For instance, McInerny[1] measured pressure levels of 139.5 dB at 820 m from the launch pad during a Titan IV rocket launch. Based on this value, the acoustic levels at 50 m from the rocket can be estimated as 187 dB, assuming linear propagation and spherical spreading. For such extreme pressure levels, the vibrations induced by the acoustic waves can cause serious damages to the launch facility or the payload, which usually contains critical instruments. In a 1971 NASA report, Timmins & Heuser[2] estimated that intense vibrations during lift-off were involved in between 30 to 60% of all the first-day launch failures during space missions. Therefore, accurately predicting the pressure levels during a rocket launch is crucial for the design of reliable space vehicles.

One simple method to predict the noise of multiple jets consists in estimating the pressure levels radiated by one single jet, and in summing the contributions of each plume as if they were isolated. Although straightforward, this approach can lead to inaccurate noise predictions as it does not consider the interactions between the jets. Notably, it is well known that the acoustic waves produced by one jet can be shielded due to their refraction and diffraction by the other plumes. This mechanism has been studied in detail by Candel et al.[3], Yu & Fratello[4] and Gerhold[5], for instance, who investigated the shielding of a harmonic source at different frequencies by a high-speed jet, and by Morris et al[6], who studied the shielding of jet noise by an adjacent jet. For two jets, shielding effects are at the origin of a shadow zone centered around the plane containing the jets, in which the pressure levels are significantly lower than those for two isolated jets, especially at high Strouhal numbers[7–9]. As observed by Kantola[8] and by Simonich et al.[9], shielding effects are stronger and occur at lower frequencies for larger values of the nozzle spacing. Moreover, the importance of shielding effects also varies with the operating conditions of the jets, including their velocity and nozzle pressure ratio. More precisely, the noise reduction achieved in the plane of the jet is weak at a low Mach number and increases with the jet velocity for subsonic jets, reaching a maximum reduction of 3 dB with respect to the noise of two isolated jets. For supersonic jets, however, the effects of the jet velocity are less clear. Simonich et al.[9] observed no significant effects of the jet velocity, whereas Kantola[8] noted a slight reduction of the importance

of shielding effects with increasing velocity at supersonic Mach numbers. This reduction was attributed to the expansion of the jet flows downstream from the convergent nozzles as a result of their underexpanded conditions.

For closely spaced twin nozzles, the jets can also interact with each other, leading to changes in the flow field, hence in the sound sources. In particular, the interactions and merging of the plumes can cause a reduction of the turbulent mixing, thus weakening the acoustic sources. For instance, in the jet midplane, Kantola[8] measured acoustic levels lower than those for two single jets. Since no shielding effects are expected in that plane, the lower levels were explained by the interactions between the jet flows, which lead to the suppression of some of the acoustic sources with respect to the configuration of two isolated single jets. In some cases, however, interactions between the jets can also be the origin of additional noise sources. For instance, for subsonic and supersonic jets, Bozak & Henderson[10] noted that the acoustic levels in the jet midplane exceed those for two isolated jets in the direction of peak noise, which was attributed to interaction effects. Similar observations were also made by Kantola[8] or Simonich et al.[9]. Moreover, at supersonic Mach numbers, an important source of interaction noise is due to coupled oscillations between the jets, which can generate intense, tonal acoustic waves[11–16]. These resonances are linked to a feedback loop which has been modelled by Tam & Seiner[17] using a vortex-sheet instability wave model. While the mechanisms involved in twin jet resonance appear to be very similar to those at the origin of screech in single supersonic jets, twin jets can have different oscillation modes and frequencies compared to single jets at the same operating conditions[11]. Furthermore, the tone levels can also be much higher than those for two isolated single screeching jets, which has been shown to be involved in the fatigue failure of certain engine parts of military aircrafts[18].

Although the interactions of twin supersonic jets have received considerable attention over the last decades, most of previous work have focused on jets at exhaust conditions typical of those for military jet engines[12,13,16,19–21]. To the best of the authors knowledge, very few studies have attempted to study twin jet interactions at conditions approaching those for rocket engines. Due to the very high speed and temperature of these jets, their shielding properties and interaction mechanisms are not well known. Notably, jets exhausting from rocket engines display very strong velocity and temperature gradients which could modify their shielding properties with respect to jets at lower speeds and temperatures. Besides, supersonic velocities can be reached in the interjet region, which could generate additional sound. Finally, while the feedback loop involved in the generation of screech tones can be suppressed at high temperatures for single jets[22], it has

been found, in some cases, to persist in the case of full-scale, heated, twin jet configurations encountered in military jet aircrafts[12,18]. This warrants further investigations on whether such a feedback loop can be observed in strongly heated, highly supersonic twin jets such as those powering rocket launchers. In order to better understand noise generation mechanisms for such supersonic jets, Piantanida & Berterretche[23] and Lambaré[24] recently performed flow and noise measurements near twin jets separated by a distance of 2.8 jet diameters at a total temperature of 2,000 K and a Mach number of 3.1. As for jets at lower speeds and temperatures, they noted the presence of a shadow zone in the plane of the jets, indicating shielding effects. They also measured an excess of sound power levels in the jet midplane with respect to the configuration of two isolated single jets, especially at low polar angles. This noise excess was discernible over a wide range of frequencies and was identified as interaction noise. Unfortunately, the mechanisms involved in its generation were not discussed due to the limited number of flow measurements available.

In the present study, large-eddy simulations of supersonic twin jet configurations are carried out at exhaust conditions very close to those considered in the study of Piantanida & Berterretche[23]. The first objective is to characterize twin jet effects, including jet shielding, mixing suppression and interaction noise, on the acoustic waves radiated by strongly heated, highly supersonic twin jets. To this end, three twin jets at a Mach number of 3.1 and a total temperature of 2,000 K are considered, with nozzle spacings of $h = 2D_e$, $2.4D_e$ and $2.8D_e$, where D_e is the nozzle diameter. Increasing the nozzle spacing is expected to move the interaction region of the jets further downstream and to change the flow properties inside this region, including the distribution and the intensity of the turbulent kinetic energy, hence modifying the acoustic sources. In addition, changing the distance between the plumes will affect the shielding properties of the twin jets, as it will modify the propagation path of the acoustic waves in the interjet region. In the simulations, as in the experiments of Piantanida & Berterrechte[23], twin jet effects will be identified by comparing the pressure levels in the near field with the levels obtained for two non-interacting single jets, which amount to twice those produced by one single jet. Using a dB scale, this is equivalent to adding 3 dB to the noise of a single jet. For that purpose, one single jet configuration is simulated at the same exit conditions as for the twin jets in order to serve as a reference. In addition, changes in the sound field will be related to changes in the flow field in order to identify the physical mechanisms involved. In particular, the distribution of turbulent kinetic energy and its modifications as a result of the jet interactions will be examined. It will help us to evaluate the

possible sources of interaction noise.

The paper is organized as follows. First, the numerical methods and parameters are introduced in section II. Then, in section III, the mean flow fields are described and the acoustic fields radiated by the twin jets are compared with those of two non-interacting single jets. Finally, concluding remarks are given in section IV and the compressible Navier-Stokes equations are detailed in Appendix A.

II. SIMULATION PARAMETERS

A. Jet parameters

In the present study, three twin jets and one single jet are simulated. Their exit conditions are identical and are based on the ones considered in the experiments carried out at the MARTEL facility by Piantanida & Berterretche[23] and Lambaré[24]. The jets are axisymmetric, have an exit Mach number $M_e = u_e/a_e$ of 3.1, where u_e is the exit velocity and a_e is the speed of sound at the nozzle exit, and their stagnation temperature T_s is 2,000 K. The twin jets have center-to-center nozzle spacings $h = 2D_e$, $2.4D_e$ and $2.8D_e$, where $D_e = 2r_0$ is the nozzle exit diameter, and are labelled Twinh2D, Twinh2.4D and Twinh2.8D, respectively. The single jet is referred to as SingleJet. The largest nozzle spacing $h = 2.8D_e$ is equal to the one considered in the experiments, and the two additional twin jets are simulated with the aim to investigate the changes in the flow and sound fields when the two plumes are placed closer to one another. The jets exhaust from axisymmetric, straight-pipe nozzles at a static pressure of $0.6p_\infty$, where $p_\infty = 10^5$ Pa is the ambient pressure. Thus, they are in an overexpanded state, as the jets in the experiments. The diameter-based Reynolds number of the single and twin jets is equal to $Re_D = u_e D_e/\nu_e = 2 \times 10^5$, where ν_e is the kinematic viscosity at the nozzle exit, computed from the Sutherland's law. In the four simulations, the ambient temperature T_∞ is set to 293 K. As a result, the acoustic Mach number of the jets is equal to $M_a = u_e/a_\infty = 4.7$, where a_∞ is the ambient speed of sound. Inside the nozzles, Blasius-like velocity profiles with a thickness of $0.15r_0$ are prescribed and weak, random perturbations are added in the boundary layers in order to trigger the transition of the shear layers from a fully laminar to a disturbed state. As proposed by Bogey et al.[25], these disturbances are Gaussian vortices of random phases and amplitudes, whose parameters are tuned in order to yield turbulence rates of 2% at the nozzle exit. Thus, the shear layers just downstream from the nozzle

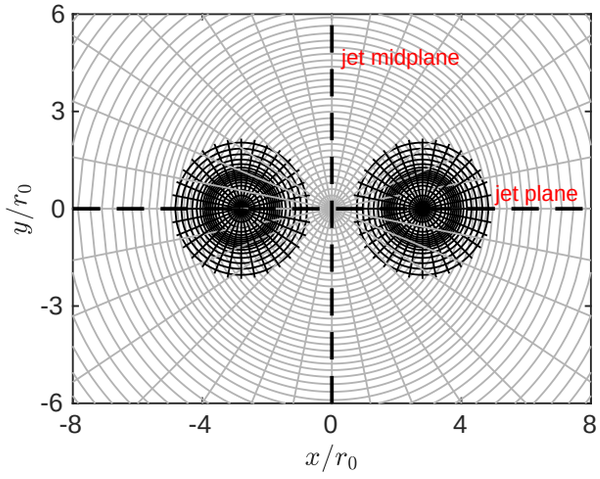

FIG. 1. Representation of the main (in gray) and secondary (in black) cylindrical grids for Twinh2.8D. One every 8 points is shown.

are in a weakly disturbed state.

B. Numerical methods

The single and twin jet simulations are performed by solving the compressible Navier-Stokes equations in cylindrical coordinates (r, θ, z) for a perfect gas, as described in Appendix A, using high-order finite-differences. For that, an in-house solver written in Fortran 90 and parallelized using OpenMP is used. This solver employs either one or several overlaid cylindrical grids and is able to simulate both single and twin jet flows. The spatial derivatives are evaluated using fourth-order eleven-point, centered, finite-difference schemes with low-dispersion properties and time integration is performed using a six-stage Runge-Kutta algorithm[26] with a formal order of 2. At the end of each time step, an 11-point, sixth-order selective filtering[27] is applied in order to damp grid-to-grid oscillations. This filtering also serves as an implicit subgrid-scale model as it relaxes turbulent kinetic energy near the grid cut-off wavenumber[28,29]. In the past, the validity of this approach has been assessed for subsonic jets[28,29], Taylor–Green vortices[30] and turbulent channel flows[31], from comparisons with the solutions of direct numerical simulations and from the examination of the filtering dissipation in the wavenumber space. Near the axis of the cylindrical grids, the azimuthal derivatives are computed using fewer points than permitted by the grids, allowing us to reduce the time-step constraint due to the use of explicit schemes[32]. In addition, the method of Mohseni & Colonius[33] is employed in order to remove the singularity at $r = 0$. In

order to prevent the development of Gibbs oscillations in the vicinity of shocks, a shock-capturing method is applied. As described in Bogey et al.[27], this method consists in applying an adaptative filtering at each time step, whose strength is defined based on a dilatation-based shock-sensor. In the past, this shock-capturing method has been used to compute the flow and sound fields of supersonic jets at similar exhaust conditions[34–38]. Finally, radiation boundary conditions[39,40] are prescribed at the inflow, outflow and radial limits of the computational domain.

While only one grid is used in the single jet computation, the twin jet simulations involve several cylindrical grids in order to take into account the non-axisymmetric geometry of the twin jet flows. As represented in Fig. 1, each of the two jets is computed on one narrow cylindrical grid while a third large grid, overlaying the two others, is used to compute the acoustic field and to allow the jets to interact in their midplane. In the following of the paper, the large and narrow grids are referred to as the main and secondary grids, respectively. This multi-domain approach allows us to use high-order finite-difference schemes to compute flows with complex geometries and has been widely used for aeroacoustics applications. Notably, very similar approaches have been adopted in the past to compute the flow and sound fields of shallow round cavities[41], rod-airfoil flows[42] as well as impinging[43] and twin supersonic jets[44,45]. In practice, the conservative flow variables are passed from one grid to another using 10th-order Lagrangian interpolations. Since the discretization in the axial direction z is identical for the three grids, the interpolations are performed for each axial position in the (r,θ) plane only. Because interpolations are performed whenever the conservative flow variables are updated, e.g. after each Runge-Kutta sub-iteration or following the application of the selective filtering, they constitute a large fraction of the total computational time. More precisely, the interpolation time has been estimated as approximately 25% of total computational time. Finally, it has been verified that the interpolation procedure does not introduce significant additional error. The verification tests included the propagation of an acoustic pulse from one cylindrical grid to the other, as well as the convection of a vortex through the interpolation zones.

C. Computational parameters

The computational domains for the four simulations extend down to $60r_0$ in the axial direction and out to $25r_0$ in the radial direction. The meshes are designed based on the results of extensive convergence studies presented by the second author in Refs.[25,46] for the LES of high-speed jets

using the same numerical methods. They yield very similar resolutions for the single and twin jets. Notably, the cylindrical grids all contain $n_\theta = 256$ points in the azimuthal direction and have identical mesh spacings in the axial direction. The axial variations of the mesh spacing Δz are shown in Fig. 2(a). It is minimum at $z = 0$, where $\Delta z = 0.014 r_0$, in order to accurately capture the fine-scale near-nozzle turbulence structures, and linearly increases with the axial coordinate up to $\Delta z = 0.05 r_0$ at $z = 60 r_0$. The radial mesh spacing Δr, represented in Fig. 2(b) at $\theta = 0$ for Twinh2.8D, is equal to $0.025 r_0$ on the jet axis and is minimum in the middle of the shear layers, at $r = h/2 \pm r_0$, where $\Delta r = 0.007 r_0$. Further outwards from the jets, it increases up to a maximum of $0.05 r_0$ for $r \geq 8 r_0$, yielding a cut-off Strouhal number of 2 for an acoustic wave discretized by four points per wavelength. This criterion is based on the recommendations of Bogey & Bailly[26] for the finite-difference schemes used. For the other twin jet simulations and for the single jet, the radial mesh spacing, not shown for brevity, is identical to that for Twinh2.8D on the jet axis, in the middle of the shear layers, as well as in the near acoustic field, leading to the same cut-off frequencies. Overall, a total number of $n_r \times n_\theta \times n_z = 640 \times 256 \times 2383 = 380$ million points are used for the single jet, while the twin jet simulations use between 541 and 563 millions points. It can be noted that the grid resolution is comparable with or finer than in state-of-the-art LES of the noise produced by hot supersonic jets[35,47,48]. The simulations are performed using a constant time step equal to $\Delta t = 0.018 a_\infty / r_0$, yielding a Courant number of $\mathrm{CFL} = \Delta t a_\infty / \Delta r_{min} = 0.37$, where $\Delta r_{min} = 0.007 r_0$ is the smallest radial mesh spacing. After an initial transient time of $1600 r_0 / u_e$, the flow and sound fields are recorded for a duration of approximately $3000 r_0 / u_e$. For the single jet, the convergence of the time-averaged statistics is improved by averaging the results over the entire circumference of the jet flow. This is not possible for the twin jets, which are not axisymmetric. As visible in Fig. 1, these configurations, however, possess two symmetry planes: the plane containing the jets, referred to as the jet plane, and the jet midplane. These symmetries are exploited in order to enhance the convergence of the statistical results. The simulations were performed using 32 core nodes of Intel 6142 Skylake with a clock frequency of 2.6 GHz and each of the twin and single jet simulations consumed approximately 100,000 and 35,000 CPU hours, respectively.

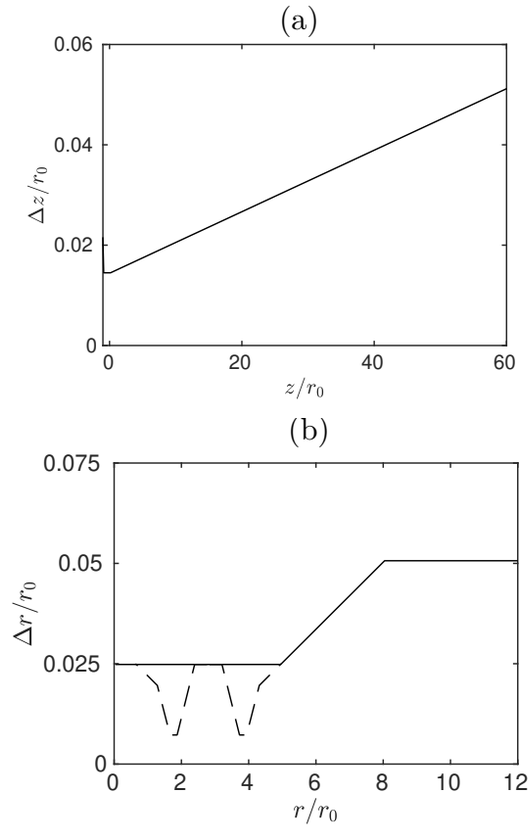

FIG. 2. Variations of the (a) axial and (b) radial mesh spacing in the plane $\theta = 0$ for Twinh2.8D; ——— main grid and – – – secondary grid.

III. RESULTS

A. Snapshots

Snapshots of the static temperature inside the jets and of the pressure fluctuations outside are provided in Fig. 3 for the three twin jets. In Fig. 3(a,c,e), in the jet plane, the plumes seem to develop independently from each others close to the nozzle exits. Further downstream, the jets interact and merge into one larger jet. This leads to the intrusion of high-temperature gases in the jet midplane, as visible in Fig. 3(b,d,f). The interactions of the jets begin at $z \simeq 15r_0$, $18r_0$ and $22r_0$ for Twinh2D, Twinh2.4D and Twinh2.8D, respectively. The position where the jets first interact is thus shifted downstream as the nozzle spacing is increased, as expected. In the near acoustic field, intense, highly directive pressure waves are radiated in the downstream direction. They are Mach waves produced by the supersonic convection of large-scale coherent structures, which constitute the main noise component for such strongly heated supersonic jets[34,47–49]. The

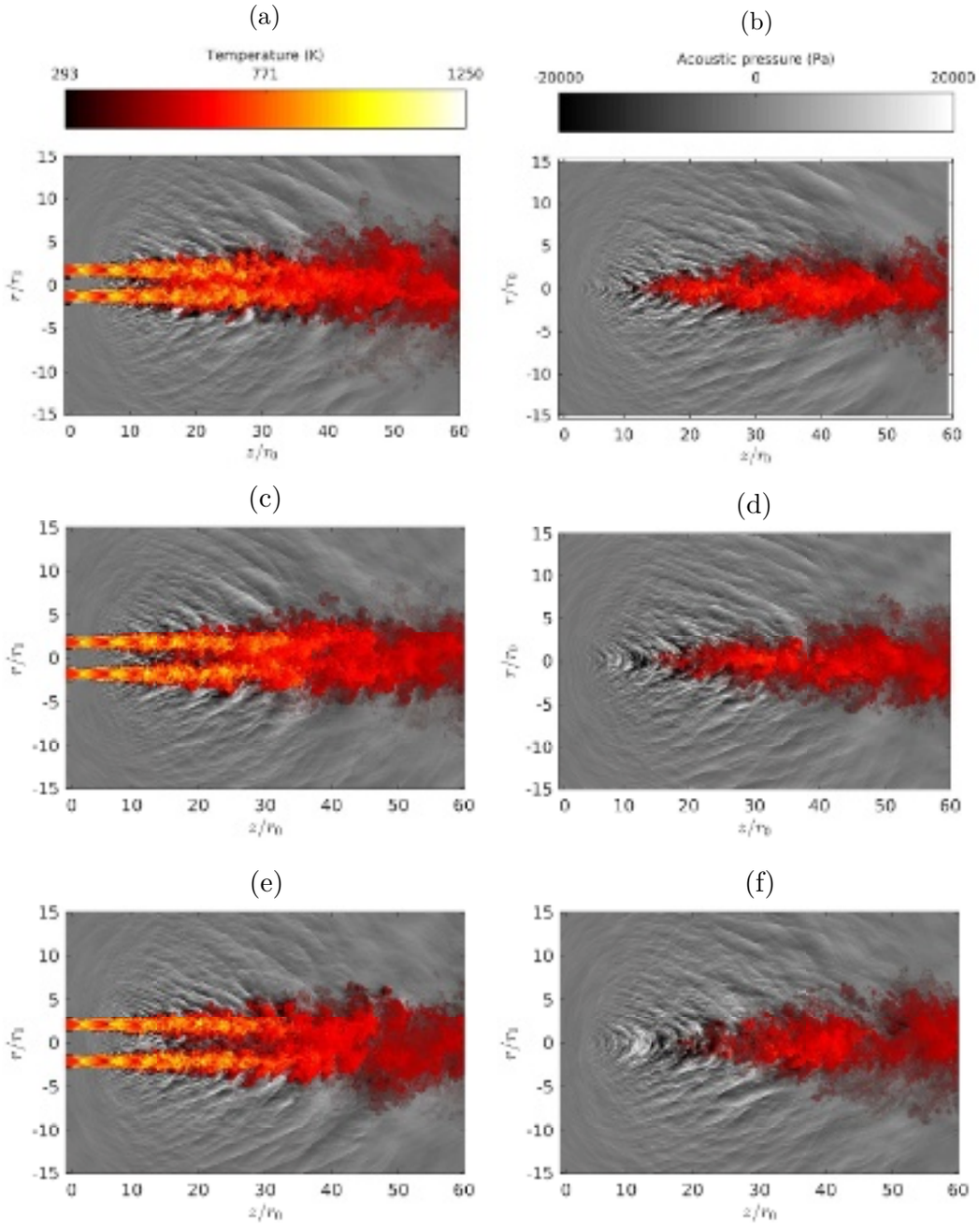

FIG. 3. Snapshots of static temperature inside the jet and of pressure fluctuations outside for (a,b) Twinh2D, (c,d) Twinh2.4D and (e,f) Twinh2.8D in the (a,c,e) jet plane and (b,d,f) jet midplane. The color scales are the same for the six representations.

propagation angle α of Mach waves can be estimated as $\alpha = \cos^{-1}(a_\infty/u_c)$, where u_c is the convection speed of the coherent structures at the origin of Mach waves. By assuming $u_c = 0.6u_e$,

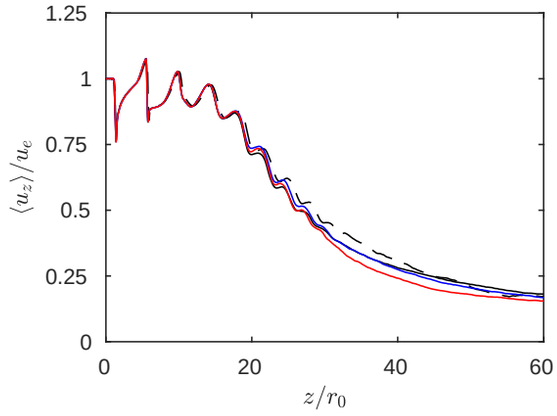

FIG. 4. Mean axial velocity on the jet axis for —— Twinh2D, —— Twinh2.4D and —— Twinh2.8D and – – – SingleJet.

this yields $\alpha = 70$ degrees, which is close to the propagation angle in the snapshots. Finally, acoustic waves are also visible in the region between the jet plumes, where the waves radiated by one particular jet impinge on the other jet.

B. Mean velocity and temperature

The axial variations of the mean axial velocity on the jet axis are plotted for the single and twin jets in Fig. 4. The centerline velocities for the twin jets are identical to those for the single jet just downstream from the nozzle exit and display marked oscillations which are due to the presence of shock cells inside the potential core because of the overexpanded conditions of the jets. Close to the nozzle, for $z \leq 20r_0$, the profiles obtained for the single and twin jet flows are identical, in agreement with the measurements of Piantanida & Berterretche[23]. At these axial locations, the jets plumes are separated from each other by a layer of very-low velocity flow and there are no interaction between the jets. Downstream from the end of the potential core, the axis velocity decreases at a faster rate for the twin jets than for the single jet. Thus, the presence of a neighboring plume does not significantly affect the structure of the shock cells in the potential core but favors the mixing of the twin jets once they interact.

The mean velocity and static temperature for the twin jets are represented in Fig. 5 on the mid-jet axis, in the center of the jet midplane. The mean velocity in Fig. 5(a) is initially close to 2% of the exit velocity but rapidly increases with the axial distance as the jets interact. Then,

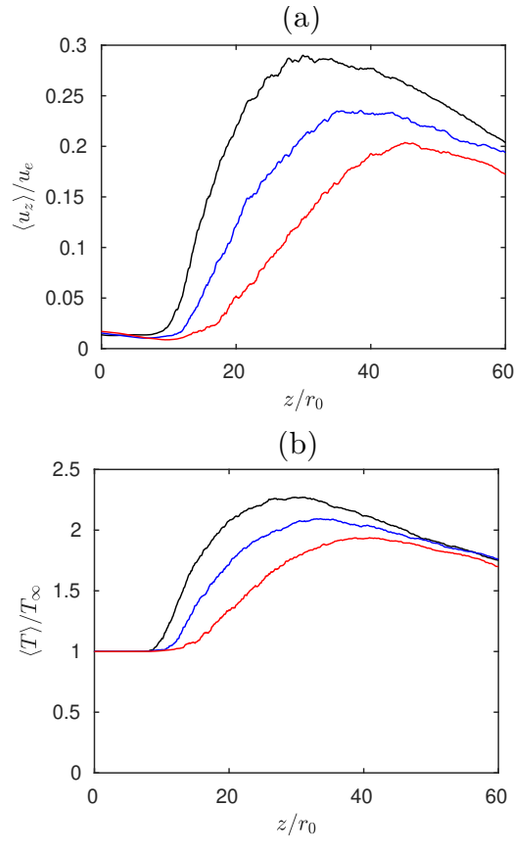

FIG. 5. Axial variations of mean (a) axial velocity and (b) static temperature in the jet midplane for ——— Twinh2D, ——— Twinh2.4D and ——— Twinh2.8D.

the mean velocity reaches a peak and decreases with the axial distance as the two twin jets merge into one single jet. The rise of the axial velocity in the jet midplane is more rapid and occurs nearer to the nozzle exit as the distance between the nozzles is reduced. Moreover, the peak mean velocity decreases with the nozzle spacing and it is equal to $0.29u_e$, $0.23u_e$ and $0.20u_e$ for Twinh2D, Twinh2.4D and Twinh2.8D, respectively. It can also be noted that these peak values correspond to $1.36a_\infty$, $1.08a_\infty$ and $0.94a_\infty$. They are thus higher than the ambient sound speed for Twinh2D and Twinh2.4D. In Fig. 5(b), the static temperature in the jet midplane is equal to the ambient temperature T_∞ near the nozzle exit and increases with the axial distance once the jets interact. It reaches peak values of $2.3T_\infty$, $2.1T_\infty$ and $1.9T_\infty$ for Twinh2D, Twinh2.4D and Twinh2.8D, respectively. Therefore, the mean static temperature in the interjet region also decreases when the nozzle spacing is larger.

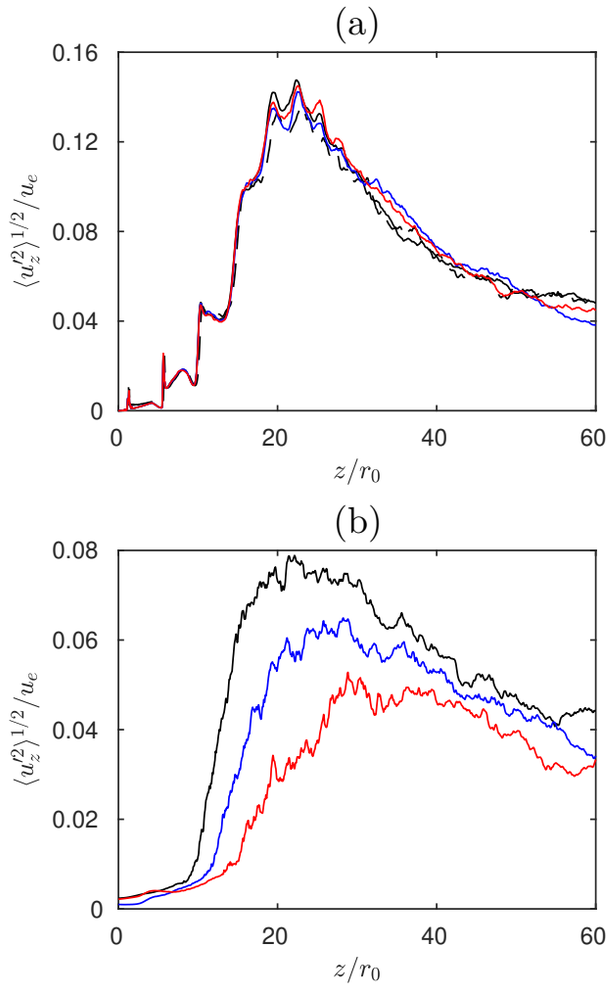

FIG. 6. RMS value of velocity fluctuations on (a) the jet axis and (b) in the center of the jet midplane for Twinh2D, Twinh2.4D, Twinh2.8D and SingleJet.

C. Turbulent fluctuations

The root-mean-square (RMS) values of the axial velocity fluctuations computed on the axis of the single and twin jet flows are plotted in Fig. 6(a). For all jets, they are initially close to 0 at $z = 0$ and sharply increase for $z \simeq 20r_0$, as the shear layers merge at the end of the potential core. They reach a maximum value of $0.15u_e$ at $z = 22r_0$ and gradually decrease. It can be noted that the RMS values of the velocity fluctuations for the twin and single jets are identical and do not depend significantly on the nozzle spacing. The turbulence rates obtained for the twin jet flows on the mid-jet axis are plotted in Fig. 6(b). They are very weak in the vicinity of the nozzle exit, but rapidly grow as the plumes interact. The maximum turbulence rate is weaker and located

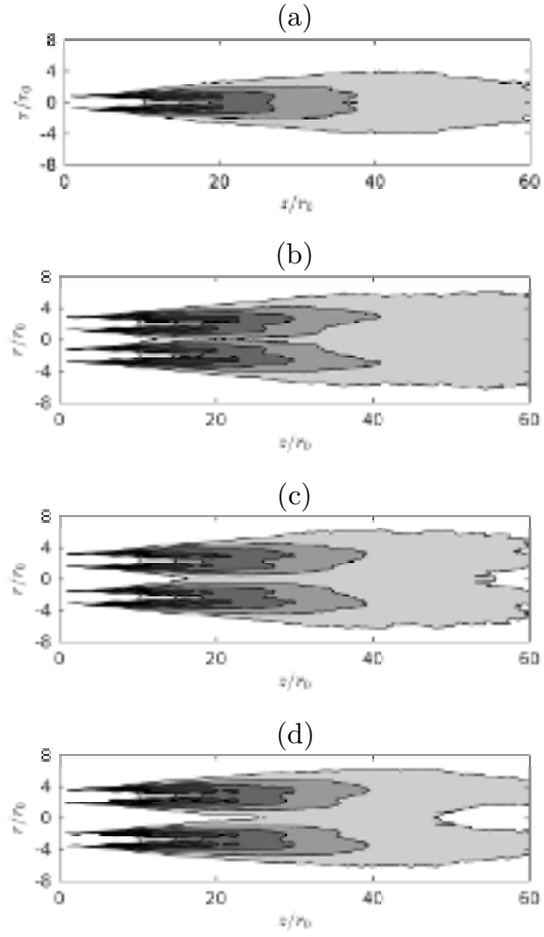

FIG. 7. RMS value of axial velocity fluctuations in the plane of the jets (a) SingleJet, (b) Twinh2D, (c) Twinh2.4D and (d) Twinh2.8D. The scales range from 0 to $0.2u_e$, from black to white.

farther from the nozzle for a larger nozzle spacing. Thus, although the turbulent fluctuations on the centerlines of the jets are poorly affected by twin jet effects, the magnitude of the turbulent fluctuations on the mid-jet axis is directly related to the nozzle spacing.

A more detailed account of the effects of twin jet interaction on the turbulence rates is provided in Fig. 7, where isocontours of the the RMS values of the velocity fluctuations are displayed for the single and twin jets. In all cases, the turbulence rates are highest inside the jet shear layers, as expected. However, the levels for the twin jets in Fig. 7(b,c,d) are not symmetric with respect to the jet axis, as is the case for the single jet in Fig. 7(a). In particular, high turbulence rates persist over a larger axial extent in the outer shear layer than in the inner one. This is clearly the case for the smallest nozzle spacing, in Fig. 7(b), but less visible for the largest one in Fig. 7(d), for which the turbulence rates are almost symmetric with respect to the jet axis. This asymmetry of the velocity

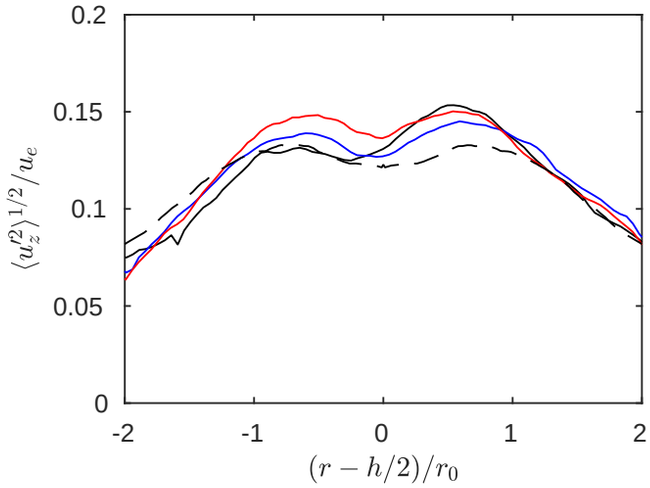

FIG. 8. Radial profiles at $z = 25r_0$ of the RMS of axial velocity fluctuations in the jet plane for —— Twinh2D, —— Twinh2.4D and —— Twinh2.8D and - - - SingleJet.

fluctuations is also observed in the simulations of Jeun et al.[50]. The effects of twin jet interaction on the jet turbulence can also be seen in Fig. 8, where radial profiles of the RMS value of the axial velocity fluctuations in the jet plane at $z = 25r_0$ are shown. This location is just downstream from the end of the potential core, close to the region of peak turbulent fluctuations. The profiles are shifted radially by half the nozzle spacing in order to compare the values of the turbulence rates in the shear layers of the twin jets. The profiles for SingleJet at the same axial position are also provided. For the twin and single jets, the RMS profiles of velocity fluctuations exhibit two peaks at $r \simeq h/2 \pm 0.5r_0$, in the center of the shear layers. The peak values of turbulence rates are higher for the twin jets than for the single jet, which suggests that the presence of a neighboring plume enhances the mixing of the jet flows. In addition, whereas the turbulence levels for Twinh28 are symmetric with respect to the jet axis as for SingleJet, those for Twinh2D and Twinh2.4D are not. For these configurations, the peak RMS value in the outer shear layers for $r + h/2 < 0$ is higher than the one in the inner shear layer for $r - h/2 > 0$, which underlines the asymmetry of the turbulent fluctuations inside the twin jets. This asymmetry is particularly marked for Twinh2D, which has the shortest nozzle spacing. Thus, the proximity of the neighboring jet tends to break the axisymmetry of the jet flow turbulence as it hinders the growth of the turbulence intensity in the inner shear layers while favoring the presence of strong levels in the outer ones. This phenomenon has also been observed by Nasr & Lai[51] for low-speed plane twin jets.

As previously noted, the turbulence levels in the inner shear layers of the twin jets increase

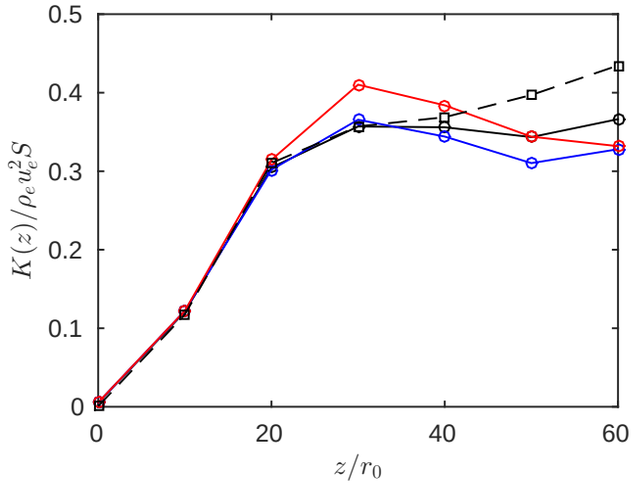

FIG. 9. Axial variations of the density of integral turbulent kinetic energy for —— Twinh2D, —— Twinh2.4D, —— Twinh2.8D and – – – two non-interacting single jets.

when the nozzle spacing is reduced, whereas those in the jet midplane decrease. In order to determine if the combination of these two opposite trends results in stronger or weaker unsteadiness for the twin jet configurations, the density of integral turbulent kinetic energy $K(z)$ is defined as the integral of the turbulent kinetic energy in planes at constant z as:

$$K(z) = \int_0^{\infty} \left[\int_0^{2\pi} \frac{1}{2} \langle \rho \rangle \left(\langle u_r'^2 \rangle + \langle u_\theta'^2 \rangle + \langle u_z'^2 \rangle \right) r \mathrm{d}\theta \right] \mathrm{d}r. \quad (1)$$

It is computed in 7 planes at axial positions ranging from $z = 0$ to $z = 60r_0$, every $10r_0$. The axial variations of the integral kinetic energy are shown in Fig. 9 for the three twin jets as well as for two isolated single jets. It is normalized by $\rho_e u_e^2 S$, where $S = \pi r_0^2$ is the initial jet cross section. The integrated kinetic energy is close to zero at the nozzle exit and rapidly increases with the axial distance. Close to the exit, for $z \leq 20r_0$, the values of $K(z)$ are very similar for the single and twin jet flows as there are little to no interactions between the jets. Farther downstream, the values obtained for the twin jets differ from those for two isolated single jets and depend on the nozzle spacing. For instance, at $z = 30r_0$, close to the end of the potential cores, the turbulent kinetic energy for the twin jets is larger than the one for two isolated single jets and displays higher values for a larger nozzle spacing. This is consistent with the profiles of turbulence rates in Fig. 8 and confirms that the presence of a neighboring jet favors the mixing of the jet flows. For $z = 50r_0$ and $z = 60r_0$, the levels of integrated turbulent kinetic energy are lower than for two non-interacting single jets. They also decrease with the nozzle spacing, which can be explained by the fact that

turbulence intensity in the jet midplane is higher when the twin jets are closer to one another, as illustrated in Fig. 6(b). Finally, it can be concluded that increasing the nozzle spacing leads to stronger fluctuations near the end of the potential core but to weaker ones downstream. Overall, Twinh2.8D is the twin jet configuration with the highest levels of turbulent kinetic energy while Twinh2.4D is the one which has the lowest levels. In the following of the paper, the present results will help us explain the effects of twin jet interactions on the acoustic waves radiated by the twin jets.

D. Near acoustic field

1. Comparisons with experimental measurements

The pressure fluctuations obtained for Twinh2.8D are compared with the acoustic measurements of Pientanida & Berterrechte[23] for a twin jet configuration with the same nozzle spacing and identical exit conditions. The acoustic measurements were performed slightly upstream from the nozzle exit, at $z = -1.3r_0$, at 6 locations displayed in Fig. 10. Two points, labelled C and F, are located in the jet plane at a distance $d = 5.2D$ from the closest jet axis. The four other ones, labelled A, B, D and E, are placed in two planes crossing the axes of the jets and parallel to the jet midplane. They are located on each side of the two jets, at a distance $d = 5.2D$ from the closest jet axis. The power spectrum densities of the pressure fluctuations are represented in Fig. 11 for Twinh2.8D. They are computed using the Welch's periodogram method by splitting the signals over windows of 2048 points with an overlap of 50%. Due to the symmetry of the twin jet configuration with respect to the jet midplane and to the plane containing the jets, the convergence of the spectra is improved by averaging the results obtained at the points labelled C and F, in Fig. 11(a) and those obtained at A, B, D and E, in Fig. 11(b). For the points C and F, in Fig. 11(a), as well as for the points A, B, D and E, in Fig. 11(b), the numerical results are in good agreement with the measurements for Strouhal numbers between 0.05 and 1. In addition, the spectra from the simulation and experiment are broadband and peak for a Strouhal number close to 0.1. At high frequencies, For $St \geq 1$, the acoustic levels obtained from the simulations are lower than in the experiments due to numerical dissipation in the vicinity of the grid cut-off Strouhal number, estimated to 2 for an acoustic wave discretized using four point per wavelength[26]. In the simulation, the overall sound pressure level (OASPL), obtained by integrating the pressure

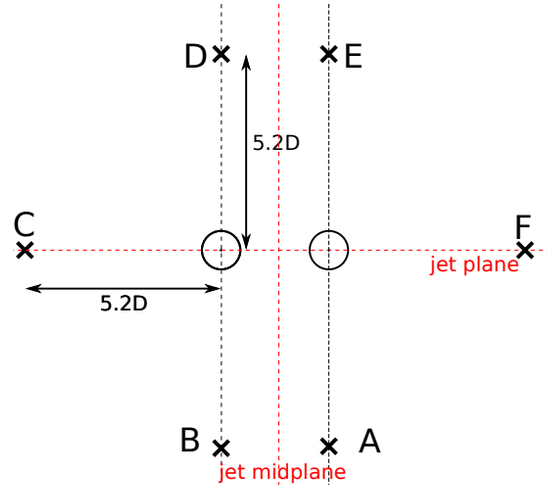

FIG. 10. Representation in the plane perpendicular to the jet axis at $z = -1.3r_0$ of the acoustic measurement points (A-F) in the experiments of Piantanida & Berterrecthe[23].

spectrum over all frequencies, is equal to 144.5 dB in the jet plane and to 145.8 dB in the planes perpendicular to the jet plane, for the measurement points A, B, D and E. These values are within 1 dB from those measured in the experiments which are of 143.7 and 145.8 dB, respectively. In the simulation and experiment, the fact that the OASPL is lower in the jet plane than in the jet midplane can be explained by acoustic shielding effects.

2. *Pressure levels between the jets*

The RMS values of the pressure fluctuations in the mid-jet axis are shown in Fig. 12(a). They rapidly increase with the axial distance and reach a peak value at $z \simeq 15r_0$, slightly before the end of the potential core. The peak value is strongest for Twinh2D and decreases with the nozzle spacing. In Fig. 12(b), the RMS values of the pressure fluctuations are normalized by $(h/D)^{1/2}$. In this way, the profiles are found to collapse reasonably well. This indicates that the pressure fluctuations are due to cylindrically-spreading Mach waves generated by the jet shear layers during the early development of the twin jets. Hence, the decrease of the pressure levels in the jet midplane with the nozzle spacing is due to the increase of the propagation distance and not to changes in the sound sources.

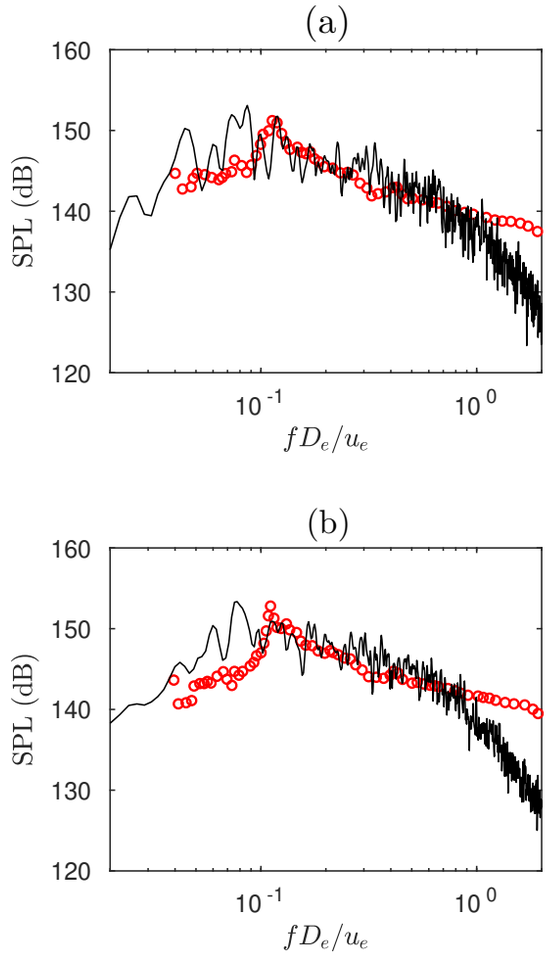

FIG. 11. Power Spectrum Densities of the sound pressure levels at $z = -1.3r_0$ for TwinH28D at a distance $d = 5.2D$ from the jet axis in (a) the jet plane and (b) in the plane containing the jet axis. The red circles indicate the experimental measurements of Piantanida & Berterretche[23] at the measurement points (a) C and (b) D.

3. *Pressure levels in the near acoustic field*

The acoustic power radiated by the twin jets is represented in Fig. 13 as a function of the axial coordinate. It is estimated by integrating the sound intensity over elementary cylindrical surfaces of radius $20r_0$ and of width $\delta z = 0.05r_0$ in the axial direction. The acoustic power for the twin and single jets have very similar shapes and display, in particular, a strong peak of noise emission at $z \simeq 35r_0$ due to Mach wave emission, as observed for supersonic single jets at comparable temperatures and Mach numbers[34,48,52]. The acoustic power is much higher for the three twin

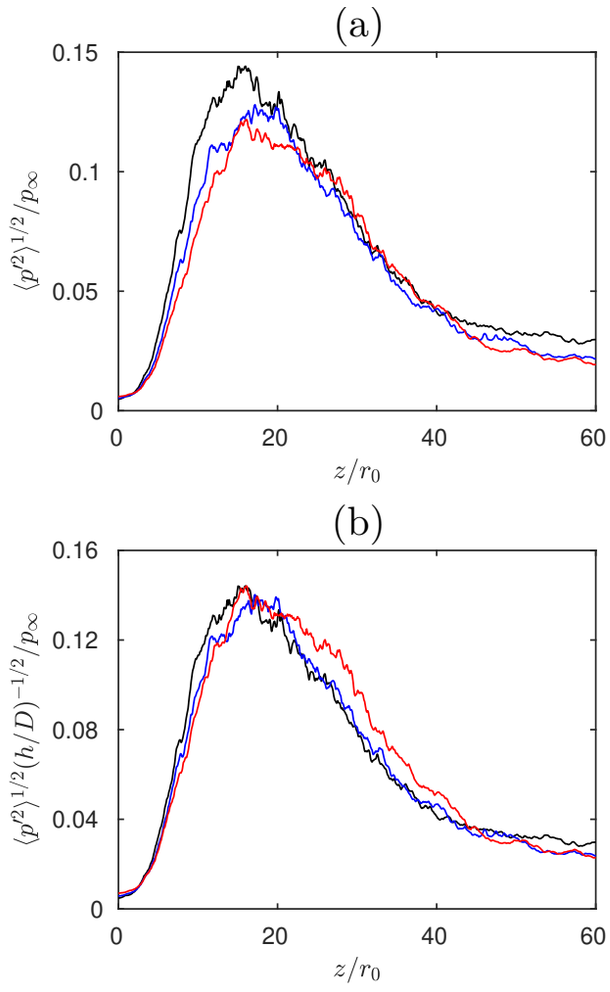

FIG. 12. RMS values of the pressure fluctuations in the jet midplane normalized by (a) p_∞ and (b) $(h/D)^{1/2}p_\infty$ for —— Twinh2D, —— Twinh2.4D and —— Twinh2.8D.

jets than the one obtained for one single jet, but lower than that for two non-interacting single jets, estimated by adding 3 dB to the noise of SingleJet. This indicates that, overall, the twin jets radiate less noise than two single jets, which can be explained by the suppression of some of the sound sources with respect to the configuration of two non-interacting jets. The acoustic power produced by the twin jets with different nozzle spacings are identical for axial positions $z \leq 30r_0$ but slightly differ for $z \geq 40r_0$. At these positions, the power density is strongest for Twinh2.8D but weakest for Twinh2.4D. Hence, its variations with the nozzle spacing are not monotonic. Interestingly, this non-monotonic trend is identical to the one identified in Fig. 9 for the total integral turbulent kinetic energy. Thus, the acoustic power generated by the twin jet flows is related to the intensity of the velocity fluctuations inside the jets.

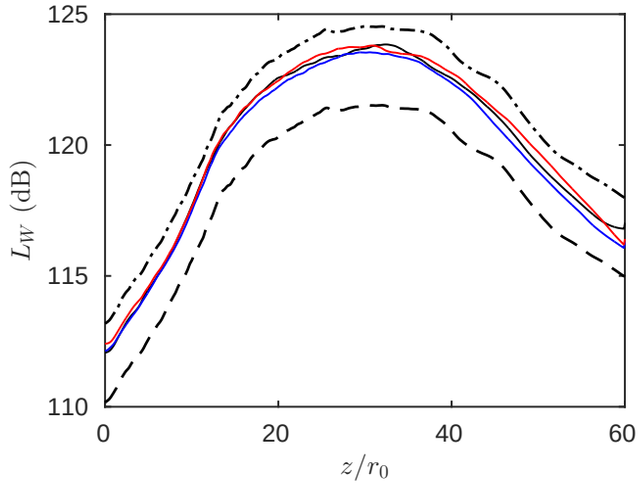

FIG. 13. Axial variations of the acoustic power estimated at $r = 20r_0$ for —— Twinh2D, —— Twinh2.4D, —— Twinh2.8D, – – – SingleJet and – · – · two non-interacting single jets.

In order to illustrate the directivity of the acoustic radiation of the twin jets in the azimuthal direction, the axial variations of the pressure levels obtained at $r = 20r_0$ in the plane of the jets and in the jet midplane are represented in Fig. 14. In the two planes, the pressure levels are 1 to 2 dB lower for the twin jet cases than for two non-interacting single jets, which can be explained by their lower total acoustic power observed in Fig. 13. The reduction of the noise levels for the twin jets is more pronounced in the plane of the jets, in Fig. 14, where shielding effects cause a further reduction of the acoustic levels as pressure waves radiated by one particular jet are refracted and diffracted by the neighboring jet, as described in refs.[3,4,8]. This leads to a redistribution of the acoustic intensity and to the reduction of the acoustic levels over a zone centered around the plane of the twin jets. For axial positions $z \simeq 30r_0$, the acoustic levels do not depend significantly on the nozzle spacing. The influence of the distance between the jets is more important downstream from the peak noise location at $z \simeq 30r_0$. At these positions, the pressure levels are higher for Twinh2D and Twinh2.8D than for Twinh2.4D, which can be explained by the fact that the two former jets have higher integral turbulent kinetic energy than Twinh2.4D, as reported before. In Fig. 14(b), the pressure levels radiated by the twin jets in their midplane are stronger than those in the plane of the jets, in agreement with the experiments of Piantanida & Berterretche[23], Kantola[8] and Bozak & Henderson[10] for jets at lower speed. These higher levels are due to the absence of shielding effects for waves radiated in the jet midplane. This is particularly noticeable between $30r_0$ and $50r_0$, where the pressure levels are very close to those for two isolated single jets. For Twinh2.8D, the

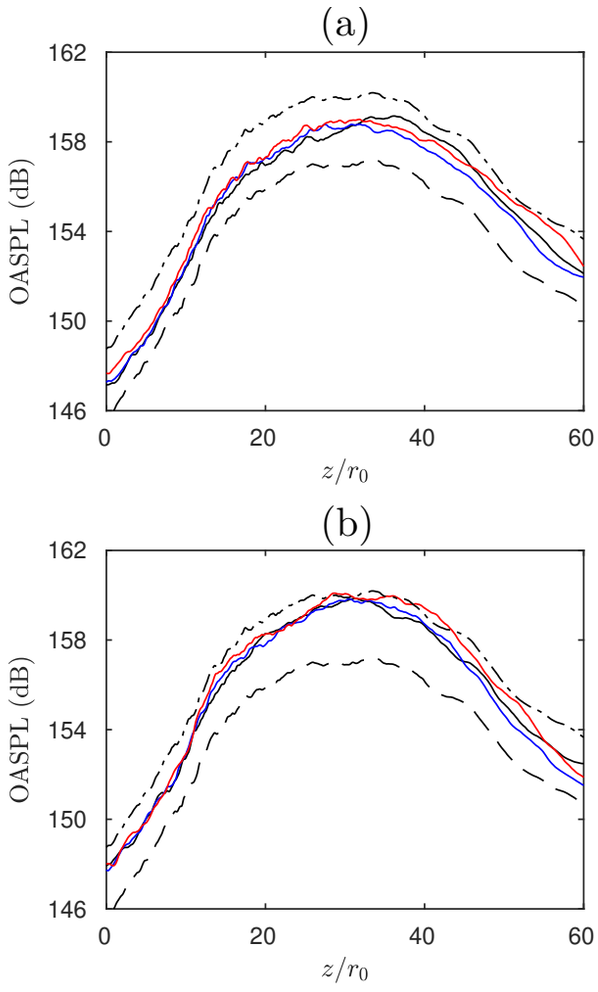

FIG. 14. Axial variations of the pressure levels at $r = 20r_0$ in (a) the plane of the jets and (b) in the jet midplane for —— Twinh2D, —— Twinh2.4D, —— Twinh2.8D, - - - SingleJet and - · - · two non-interacting single jets.

acoustic levels even exceed those for two non-interacting single jets, which suggests that additional interaction noise is generated by the twin jets. This is investigated into further details in what follows.

4. Pressure spectra

The power spectrum densities (PSD) of the pressure fluctuations at $r = 20r_0$ and $z = 0$ are shown in Fig. 15. In the plane of the jets, in Fig. 15(a), as well as in the jet midplane, in Fig. 15(b), the spectra for the twin jets have a shape very similar to that of two non-interacting jets. They

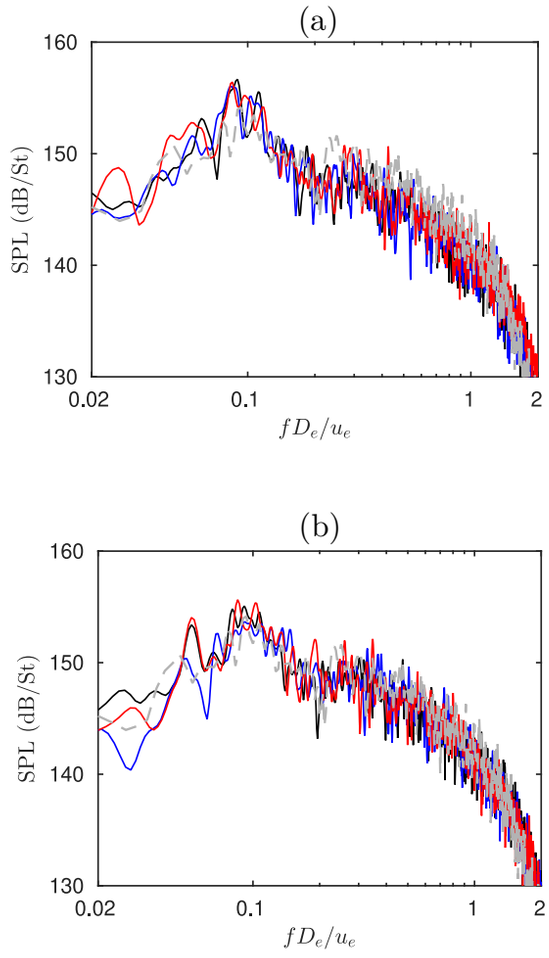

FIG. 15. Power spectrum densities of the pressure fluctuations at $r = 20r_0$ and $z = 0$ in the (a) jet plane and (b) jet midplane for ——— Twinh2D, ——— Twinh2.4D, ——— Twinh2.8D and - - - two non-interacting single jets.

display, in particular, a hump centered around a Strouhal number $S = fD_e/u_e$ of 0.1, with f the frequency, due to broadband shock associated noise (BBSAN). This noise component is generated by the interaction of the shear-layer turbulence with the shock cells inside the jets and constitutes a major part of the noise radiated in the upstream direction for shock-containing supersonic jets[53,54]. In the plane of the twin jets, the level of BBSAN is 1 to 2 dB higher than that for the two non-interacting jets, which can be explained by the fact that the shear layers of the twin jets exhibit higher turbulence rates than those of the single jet in Fig. 7. In the jet midplane in Fig. 15(b), the magnitude of the BBSAN does not seem to depend on the nozzle spacing. Moreover, the acoustic levels in the jet plane in Fig. 14(a) are lower than those for two non-interacing jets for Strouhal

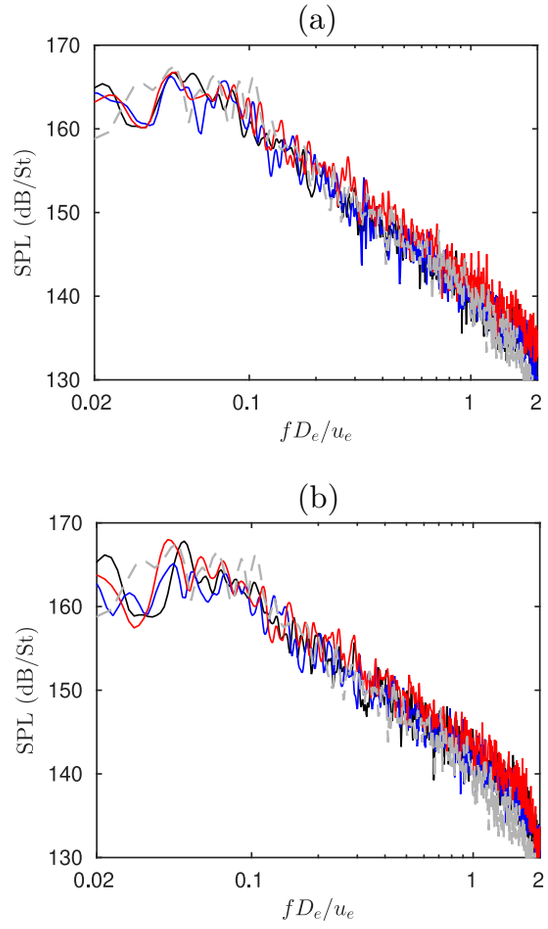

FIG. 16. Power spectrum densities of the pressure fluctuations at $r = 20r_0$ and $z = 50r_0$ in the (a) jet plane and (b) jet midplane for ——— Twinh2D, ——— Twinh2.4D, ——— Twinh2.8D and - - - two non-interacting jets.

numbers higher than 0.3. Such an observation is typical of shielding effects in twin supersonic jets as reported, for instance, in the study of Kantola[8]. Finally, the spectra of the twin and single jets do not display any notable tonal component, suggesting that there is no significant screech or twin jet resonance. This is consistent with the experimental measurements of Piantanida & Berterretche[23], and is likely due to the high temperature of the jets. Indeed, as reported by Tam et al.[22], the intensity of the screech component diminish and can disappear at a very high temperature.

The spectra of the pressure fluctuations radiated in the downstream direction, for $r = 20r_0$ and $z = 50r_0$ are represented in Fig. 16. In the plane of the jets, in Fig. 16(a), as well as in the jet midplane, in Fig. 16(b), the spectra for the single and twin jets peak at a Strouhal number of 0.05

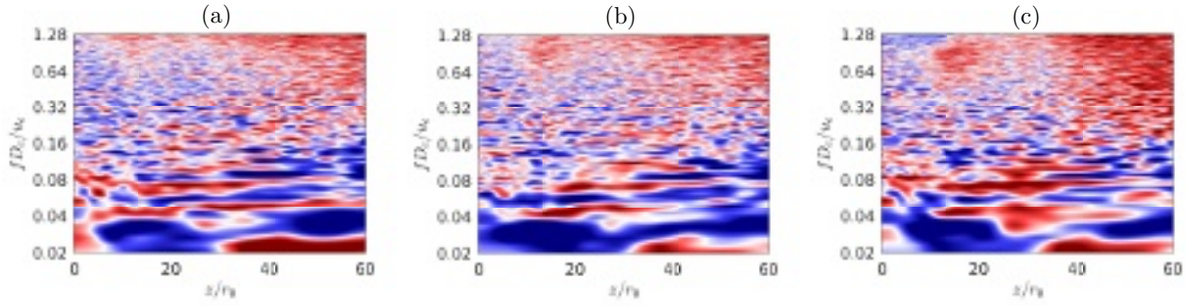

FIG. 17. Difference between the PSD at $r = 20r_0$ for (a) Twinh2D, (b) Twinh2.4D, (c) Twinh2.8D and two non-interacing jets in the jet midplane. The color scale ranges between $\pm$ 5 dB, from blue to red.

and have a shape typical of the spectra measured at low polar angles in the acoustic field of high-temperature supersonic jets[35,48]. Unlike at $z = 0$ in Fig. 15, no clear shielding effects appear in the jet plane in Fig. 16(a) as the spectra for the twin jets are close to those for two isolated jets over a wide range of frequencies. For Strouhal numbers higher than 0.1, the pressure levels of the twin jets even exceed those for two non-interacting single jets, especially at high frequencies, which suggests that the twin jets generate interaction noise. The noise excess is more significant in the jet midplane than in the jet plane. It is also strongest for Twinh2.8D, for which the acoustic levels in the jet midplane are approximately 3 dB higher than those for two isolated jets for a Strouhal number of $fD/u_j \simeq 0.5$.

The differences between the PSD of the pressure fluctuations at $r = 20r_0$ obtained for the twin jets and for two non-interacting single jets are represented in Fig. 17 as a function of the axial position and of the Strouhal number. For the three nozzle spacings, the acoustic levels for the twin jets are higher than for the two non-interacting jets at positions downstream from $z \simeq 40r_0$ and for Strouhal numbers higher than approximately 0.16, which can be explained by the generation of interaction noise. Such a noise excess is consistent with the experimental measurements carried out by Piantanida & Berterretche[23] in the far acoustic field of a twin jet with conditions very close to those of Twinh2.8D. It is stronger for a larger nozzle spacing and it is noticeable over a wider extent of the acoustic field. This can be related to the observation in Fig. 8 that the turbulence rates in the inner shear layers of the twin jets are higher for larger values of the nozzle spacing and suggests that the intensity of interaction noise is linked to that of the turbulent fluctuations in the region where the twin jets interact.

IV. CONCLUSION

The noise and interactions of strongly heated supersonic twin jets are investigated in the present study by performing numerical simulations of twin jets separated by distances of $2D_e$, $2.4D_e$ and $2.8D_e$, where D_e is the nozzle diameter. A single jet with the same exit conditions is also computed and serves as a reference to identify interaction mechanisms in the jet flow and sound fields. Close to the nozzle exit, the mean velocity and turbulence rates on the axis of the twin jets are identical to those for the single jets as there are little to no interaction effects. Further downstream, the twin jets begin to interact at a position located near the end of their potential cores and then merge into one single, larger jet. Once the twin jets interact, their shear layers display higher turbulence levels than those of the single jets, indicating that the presence of a neighboring plume favors the mixing of the jets. Besides, unlike for the single jet flow, the radial distribution of turbulent kinetic energy in the twin jets is not symmetric with respect to the jet axis, as the turbulence rates in the inner shear layers are lower than in the outer one. The turbulence rates in the inner shear layers are also higher for a larger nozzle spacing, whereas those in the jet midplane are lower.

In the near pressure field, the acoustic power radiated by the twin jets is 1 to 2 dB lower than that for two non-interacting single jets at all polar angles, suggesting that the interaction of the jet flows leads to the suppression of some of the sound sources with respect to the reference configuration. The noise reduction is largest for the twin jet with the intermediate nozzle spacing $h = 2.4D_e$, which is the one for which the total integrated turbulent kinetic energy is lowest. In addition, the decrease of the pressure levels mostly affects the high frequencies and is particularly important in the plane containing the jets, due to the refraction and diffraction of the acoustic waves by the neighboring plume, i.e. to shielding effects. Despite the global noise reduction, the noise of the twin jets exceeds that for two non-interacting jets for certain angles and frequencies. Notably, the broadband shock-associated noise component for the twin jets is 1 to 2 dB stronger than that for two non-interacting single jets. This is also the case for the acoustic waves radiated at low polar angles, especially in the high-frequency range, suggesting that additional noise is generated by the interaction of the twin jets. This additional noise component is more prominent in the jet midplane, increases with the nozzle spacing and appears to be related to the turbulence intensity in the interaction region of the twin jets.

The observation of the generation of interaction noise for strongly heated supersonic twin jets is one of the main results of the present paper. While the generation of interaction noise has been

observed in previous studies of twin jets at different Mach numbers[8,10] the generation mechanisms involved have not been documented. Thus, additional measurements and simulations would be useful in order to characterize the noise excess due to twin jet interactions over a wide range of jet operating conditions.

Appendix A: Governing equations

In the simulations, the full compressible Navier-Stokes equations are solved in cylindrical coordinates (r,θ,z) in conservative form. These equations describe the conservation of mass, momentum and energy for a perfect gas. They can be written as :

$$\begin{aligned}\frac{\partial U}{\partial t}+\left(\frac{1}{r}\frac{\partial rE_e}{\partial r}+\frac{1}{r}\frac{\partial F_e}{\partial \theta}+\frac{\partial G_e}{\partial z}\right)\\ -\left(\frac{1}{r}\frac{\partial rE_v}{\partial r}+\frac{1}{r}\frac{\partial F_v}{\partial \theta}+\frac{\partial G_v}{\partial z}\right)+\frac{B_e}{r}-\frac{B_v}{r}=0,\end{aligned} \tag{A1}$$

where $U=(\rho,\rho u_r,\rho u_\theta,\rho u_z,\rho e)$ is the vector of the conservative variables, with ρ the density, u_r, u_θ and u_z the three components of the velocity and $\rho e = p/(\gamma-1)+1/2\rho(u_r^2+u_\theta^2+u_z^2)$ the energy.

The quantities E_e, F_e and G_e in (A1) are defined as :

$$E_e=\begin{pmatrix}\rho u_r\\ p+\rho u_r^2\\ \rho u_r u_\theta\\ \rho u_r u_z\\ (\rho e+p)u_r\end{pmatrix}, \tag{A2}$$

$$F_e=\begin{pmatrix}\rho u_\theta\\ \rho u_r u_\theta\\ p+\rho u_\theta^2\\ \rho u_\theta u_z\\ (\rho e+p)u_\theta\end{pmatrix} \text{ and } G_e=\begin{pmatrix}\rho u_z\\ \rho u_r u_z\\ \rho u_\theta u_z\\ p+\rho u_z^2\\ (\rho e+p)u_z\end{pmatrix}, \tag{A3}$$

while E_v, F_v et G_v are defined as

$$E_v = \begin{pmatrix} 0 \\ \tau_{rr} \\ \tau_{r\theta} \\ \tau_{rz} \\ u_r\tau_{rr} + u_\theta\tau_{r\theta} + u_z\tau_{rz} - q_r \end{pmatrix}, \qquad F_v = \begin{pmatrix} 0 \\ \tau_{r\theta} \\ \tau_{\theta\theta} \\ \tau_{z\theta} \\ u_r\tau_{r\theta} + u_\theta\tau_{\theta\theta} + u_z\tau_{z\theta} - q_\theta \end{pmatrix}, \tag{A4}$$

and

$$G_v = \begin{pmatrix} 0 \\ \tau_{rz} \\ \tau_{z\theta} \\ \tau_{zz} \\ u_r\tau_{zz} + u_\theta\tau_{z\theta} + u_z\tau_{zz} - q_z \end{pmatrix}, \tag{A5}$$

where τ_{rr}, $\tau_{\theta\theta}$, τ_{zz}, $\tau_{r\theta}$ and τ_{rz} are the components of the viscous stress tensor in cylindrical coordinates, defined as

$$\begin{cases} \tau_{rr} &= 2\mu(T)\frac{\partial u_r}{\partial r} - \frac{2}{3}\mu(T)\left(\frac{1}{r}\frac{\partial r u_r}{\partial r} + \frac{1}{r}\frac{\partial u_\theta}{\partial \theta} + \frac{\partial u_z}{\partial z}\right) \\ \tau_{\theta\theta} &= 2\mu(T)\left(\frac{1}{r}\frac{\partial u_\theta}{\partial \theta} + \frac{u_r}{r}\right) - \frac{2}{3}\mu(T)\left(\frac{1}{r}\frac{\partial r u_r}{\partial r} + \frac{1}{r}\frac{\partial u_\theta}{\partial \theta} + \frac{\partial u_z}{\partial z}\right) \\ \tau_{zz} &= 2\mu(T)\frac{\partial u_z}{\partial z} - \frac{2}{3}\mu(T)\left(\frac{1}{r}\frac{\partial r u_r}{\partial r} + \frac{1}{r}\frac{\partial u_\theta}{\partial \theta} + \frac{\partial u_z}{\partial z}\right) \\ \tau_{r\theta} &= \mu(T)\left(\frac{1}{r}\frac{\partial u_r}{\partial \theta} + \frac{\partial u_\theta}{\partial \theta} - \frac{u_r}{r}\right) \\ \tau_{rz} &= \mu(T)\left(\frac{\partial u_r}{\partial z} + \frac{\partial u_z}{\partial r}\right) \\ \tau_{z\theta} &= \mu(T)\left(\frac{1}{r}\frac{\partial u_z}{\partial \theta} + \frac{\partial u_\theta}{\partial z}\right) \end{cases} \tag{A6}$$

The terms B_e and B_v are defined as

$$B_e = \begin{pmatrix} 0 \\ \rho u_\theta^2 + p \\ \rho u_r u_\theta \\ 0 \\ 0 \end{pmatrix} \text{ and } B_v = \begin{pmatrix} 0 \\ -\tau_{\theta\theta} \\ \tau_{r\theta} \\ 0 \\ 0 \end{pmatrix}, \tag{A7}$$

and the heat flux $\mathbf{q} = (q_r, q_\theta, q_z)$ is linked to the temperature gradient ∇T through the Fourier's law

$$\mathbf{q} = -\frac{\mu(T) c_p}{\mathrm{Pr}} \nabla \mathbf{T}, \tag{A8}$$

where $\mathrm{Pr} = 0.7$ is the Prandtl number and $\mu_T(\mathrm{T})$ is the dynamic viscosity computed from the static temperature using the Sutherland's law :

$$\mu(T) = \mu_0 \left(\frac{T}{T_0}\right)^{3/2} \frac{T_0 + S}{T + S}, \tag{A9}$$

where $S = 111$ K, $T_0 = 273$ K, and $\mu_0 = 1.716 \times 10^{-5}$ kg·m^{-1}·s^{-1}.

ACKNOWLEDGEMENTS

The authors gratefully aknowledge the Centre National d'Études Spatiales (CNES) for funding the post-doctoral fellowship of the first author, with Dr Hadrien Lambaré as technical supervisor. This work was granted access to the HPC resources of PMCS2I (Pôle de Modélisation et de Calcul en Sciences de l'Ingénieur et de l'Information) of Ecole Centrale de Lyon, PSMN (Pôle Scientifique de Modélisation Numérique) of ENS de Lyon and P2CHPD (Pôle de Calcul Hautes Performances Dédiés) of Université Lyon I, members of FLMSN (Fédération Lyonnaise de Modélisation et Sciences Numériques), partner of EQUIPEX EQUIP@MESO, and to the resources of IDRIS (Institut du Développement et des Ressources en Informatique Scientifique) under the allocation 2020-2a0204 made by GENCI (Grand Equipement National de Calcul Intensif). It was performed within the framework of the Labex CeLyA of Université de Lyon, within the programme 'Investissements d'Avenir' (ANR-10-LABX-0060/ANR-16-IDEX-0005) operated by the French National Research Agency (ANR).

DATA AVAILABILITY

The data that support the findings of this study are available from the corresponding author upon reasonable request.

REFERENCES

[1]S. A. McInerny, "Launch vehicle acoustics. II - Statistics of the time domain data," J. Aircr. **33**, 518–523 (1996).

[2]A. R. Timmins and R. E. Heuser, "A study of first-day space malfunctions," Tech. Rep. NASA-TN-D-6474, G-1038 (NASA, 1971).

[3]S. M. Candel, M. Julliand, and A. Julienne, "Shielding and scattering by a jet flow," AIAA paper 1976-545 (1976), 10.2514/6.1976-545.

[4]J. C. Yu and D. J. Fratello, "Measurement of acoustic shielding by a turbulent jet," J. Sound Vib. **98**, 183 – 212 (1985).

[5]C. H. Gerhold, "Analytical model of jet shielding," AIAA J. **21**, 694–698 (1983).

[6]P. Morris, W. Richarz, and H. Ribner, "Reduction of peak jet noise using jet refraction," Journal of Sound and Vibration **29**, 443 – 455 (1973).

[7]W. V. Bhat, "Experimental investigation of noise reduction from two parallel-flow jets," AIAA J. **16**, 1160–1167 (1978).

[8]R. Kantola, "Acoustic properties of heated twin jets," J. Sound Vib. **79**, 79 – 106 (1981).

[9]J. C. Simonich, R. K. Amiet, and R. H. Schlinker, "Jet shielding of jet noise," Tech. Rep. NASA-CR-3966 (NASA, 1986).

[10]R. F. Bozak and B. S. Henderson, "Aeroacoustics experiments with twin jets," AIAA Paper 2011-2790 (2011), 10.2514/6.2011-2790.

[11]T. D. Norum and J. G. Shearin, "Dynamic loads on twin jet exhaust nozzles due to shock noise," J. Airc. **23**, 728–729 (1986).

[12]J. M. Seiner, J. C. Manning, and M. K. Ponton, "Dynamic pressure loads associated with twin supersonic plume resonance," AIAA J. **26**, 954–960 (1988).

[13]M. B. Alkislar, A. Krothapalli, I. Choutapalli, and L. Lourenco, "Structure of supersonic twin jets," AIAA J. **43**, 2309–2318 (2005).

[14]G. Raman, P. Panickar, and C. Kanthasamy, "Aeroacoustics of twin supersonic jets: a review," Int. J. Aeroacoust. **11**, 957–984 (2012).

[15]G. Bell, J. Soria, D. Honnery, and D. Edgington-Mitchell, "An experimental investigation of coupled underexpanded supersonic twin-jets," Exp. Fluids **59** (2018), 10.1007/s00348-018-2593-1.

[16]T. Knast, G. Bell, M. Wong, C. M. Leb, J. Soria, D. R. Honnery, and D. Edgington-Mitchell, "Coupling modes of an underexpanded twin axisymmetric jet," AIAA J. **56**, 3524–3535 (2018).

[17]C. K. W. Tam and J. M. Seiner, "Analysis of twin supersonic plume resonance," AIAA Paper 1987-2695 (1987), 10.2514/6.1987-2695.

[18]D. E. Berndt, "Dynamic pressure fluctuations in the internozzle region of a twin-jet nacelle," in *Aerospace Congress and Exposition* (SAE International, 1984).

[19]C.-W. Kuo, J. Cluts, and M. Samimy, "Exploring physics and control of twin supersonic circular jets," Int. J. Aeroacoust. **55**, 68–85 (2017).

[20]J. Jeun, G. J. Wu, and S. K. Lele, "Towards large-eddy simulations of twin rectangular jets including screech," AIAA Paper 2020-0998 (2020), 10.2514/6.2020-0998.

[21]A. Esfahani, N. Webb, and M. Samimy, "Coupling modes in supersonic twin rectangular jets," AIAA paper 2021-1282 (2021), 10.2514/6.2021-12924.

[22]C. K. W. Tam, K. K. Ahuja, and R. R. Jones, "Screech tones from free and ducted supersonic jets," AIAA J. **32**, 917–922 (1994).

[23]P. Piantanida, S. & Berterretche, "Acoustic characterisation of two parallel supersonic jets," (Inter Noise 2019, June 16-19, Madrid, 2019).

[24]H. Lambaré, "Experimental study of the aeroacoustic interaction between two supersonic hot jets," J. Acoust. Soc. Am. **142**, 2490–2490 (2017).

[25]C. Bogey, O. Marsden, and C. Bailly, "Large-eddy simulation of the flow and acoustic fields of a Reynolds number 10^5 subsonic jet with tripped exit boundary layers," Phys. Fluids **23**, 035104 (2011).

[26]C. Bogey and C. Bailly, "A family of low dispersive and low dissipative explicit schemes for flow and noise computations," J. Comput. Phys. **194**, 194 – 214 (2004).

[27]C. Bogey, N. de Cacqueray, and C. Bailly, "A shock-capturing methodology based on adaptative spatial filtering for high-order non-linear computations," J. Comput. Phys. **228**, 1447 – 1465 (2009).

[28]C. Bogey and C. Bailly, "Computation of a high Reynolds number jet and its radiated noise using large eddy simulation based on explicit filtering," Comput. & Fluids **35**, 1344 – 1358 (2006).

[29]C. Bogey and C. Bailly, "Turbulence and energy budget in a self-preserving round jet: direct evaluation using large eddy simulation," J. Fluid Mech. **627**, 129–160 (2009).

[30]D. Fauconnier, C. Bogey, and E. Dick, "On the performance of relaxation filtering for large-eddy simulation," J. Turbul. **14**, 22–49 (2013).

[31]F. Kremer and C. Bogey, "Large-eddy simulation of turbulent channel flow using relaxation filtering: Resolution requirement and Reynolds number effects," Comput. and Fluids **116**, 17–28 (2015).

[32]C. Bogey, N. de Cacqueray, and C. Bailly, "Finite differences for coarse azimuthal discretization and for reduction of effective resolution near origin of cylindrical flow equations," J. Comput. Phys. **230**, 1134 – 1146 (2011).

[33]K. Mohseni and T. Colonius, "Numerical treatment of polar coordinate singularities," J. Comput. Phys. **157**, 787 – 795 (2000).

[34]N. de Cacqueray, C. Bogey, and C. Bailly, "Investigation of a high-mach-Number overexpanded jet using large-eddy simulation," AIAA J. **49**, 2171–2182 (2011).

[35]N. de Cacqueray and C. Bogey, "Noise of an overexpanded Mach 3.3 jet: Non-linear propagation effects and correlations with flow," Int. J. Aeroacoust. **13**, 607–632 (2014).

[36]P. Pineau and C. Bogey, "Steepened Mach waves near supersonic jets: study of azimuthal structure and generation process using conditional averages," J. Fluid Mech. **880**, 594–619 (2019).

[37]P. Pineau and C. Bogey, "Temperature effects on convection speed and steepened waves of temporally developing supersonic jets," AIAA J. **58**, 1227–1239 (2020).

[38]P. Pineau and C. Bogey, "Numerical investigation of wave steepening and shock coalescence near a cold mach 3 jet," JASA **149**, 357–370 (2021).

[39]C. K. W. Tam and Z. Dong, "Radiation and outflow boundary conditions for direct computation of acoustic and flow disturbances in a nonuniform mean flow," J. Comput. Acoust. **04**, 175–201 (1996).

[40]C. Bogey and C. Bailly, "Three-dimensional non-reflective boundary conditions for acoustic simulations: far field formulation and validation test cases," Acta Acustica **88**, 463–471 (2002).

[41]O. Marsden, C. Bogey, and C. Bailly, "Investigation of flow features around shallow round cavities subject to subsonic grazing flow," Phys. Fluids **24**, 125107 (2012).

[42]F. Daude, J. Berland, T. Emmert, P. Lafon, F. Crouzet, and C. Bailly, "A high-order finite-difference algorithm for direct computation of aerodynamic sound," Computers & Fluids **61**, 46–63 (2012).

[43]R. Gojon and C. Bogey, "Effects of the angle of impact on the aeroacoustic feedback mechanism in supersonic impinging planar jets," Int. J. Aeroacoust. **18**, 258–278 (2019).

[44]J. Gao, X. Xu, and X. Li, "Numerical simulation of supersonic twin-jet noise with high-order finite difference scheme," AIAA J. **56**, 290–300 (2018).

[45]K. Goparaju, D. Unnikrishnan, and D. V. Gaitonde, "Acoustic characteristics of a supersonic twin-jet configuration," AIAA paper 2018-3304 (2018), 10.2514/6.2018-3304.

[46]C. Bogey, "Grid sensitivity of flow field and noise of high-reynolds-number jets computed by large-eddy simulation," Int. J. Aeroacoust. **17**, 299–424 (2018).

[47]T. Nonomura, H. Nakano, Y. Ozawa, D. Terakado, M. Yamamoto, K. Fujii, and A. Oyama, "Large eddy simulation of acoustic waves generated from a hot supersonic jet," Shock Waves **29**, 1133–1154 (2019).

[48]A. Langenais, F. Vuillot, J. Troyes, and C. Bailly, "Accurate simulation of the noise generated by a hot supersonic jet including turbulence tripping and nonlinear acoustic propagation," Phys. Fluids **31**, 016105 (2019).

[49]P. Pineau and C. Bogey, "Links between steepened mach waves and coherent structures for a supersonic jet," AIAA J. **59**, 1673–1681 (2021).

[50]J. Jeun, G. J. Wu, S. K. Lele, A. Karnam, F. Baier, and E. F. Gutmark, "Twin rectangular jet screech and coupling: Numerical study and validation," AIAA Paper 2021-1290 (2021), 10.2514/6.2021-1290.

[51]A. Nasr and J. Lai, "Two parallel plane jets: mean flow and effects of acoustic excitation," Exp. Fluids **22**, 251–260 (1997).

[52]J. Varnier and D. Gély, "Caractérisation aérodynamique et acoustique d'un jet fortement supersonique en présence d'un obstacle plan," Tech. Rep. ONERA Rept. RT-112/3643 (not published) (ONERA, 1998).

[53]C. Tam and H. Tanna, "Shock associated noise of supersonic jets from convergent-divergent nozzles," J. Sound Vib. **81**, 337 – 358 (1982).

[54]C. K. W. Tam, "Supersonic jet noise," Ann. Rev. Fluid Mech. **27**, 17–43 (1995).

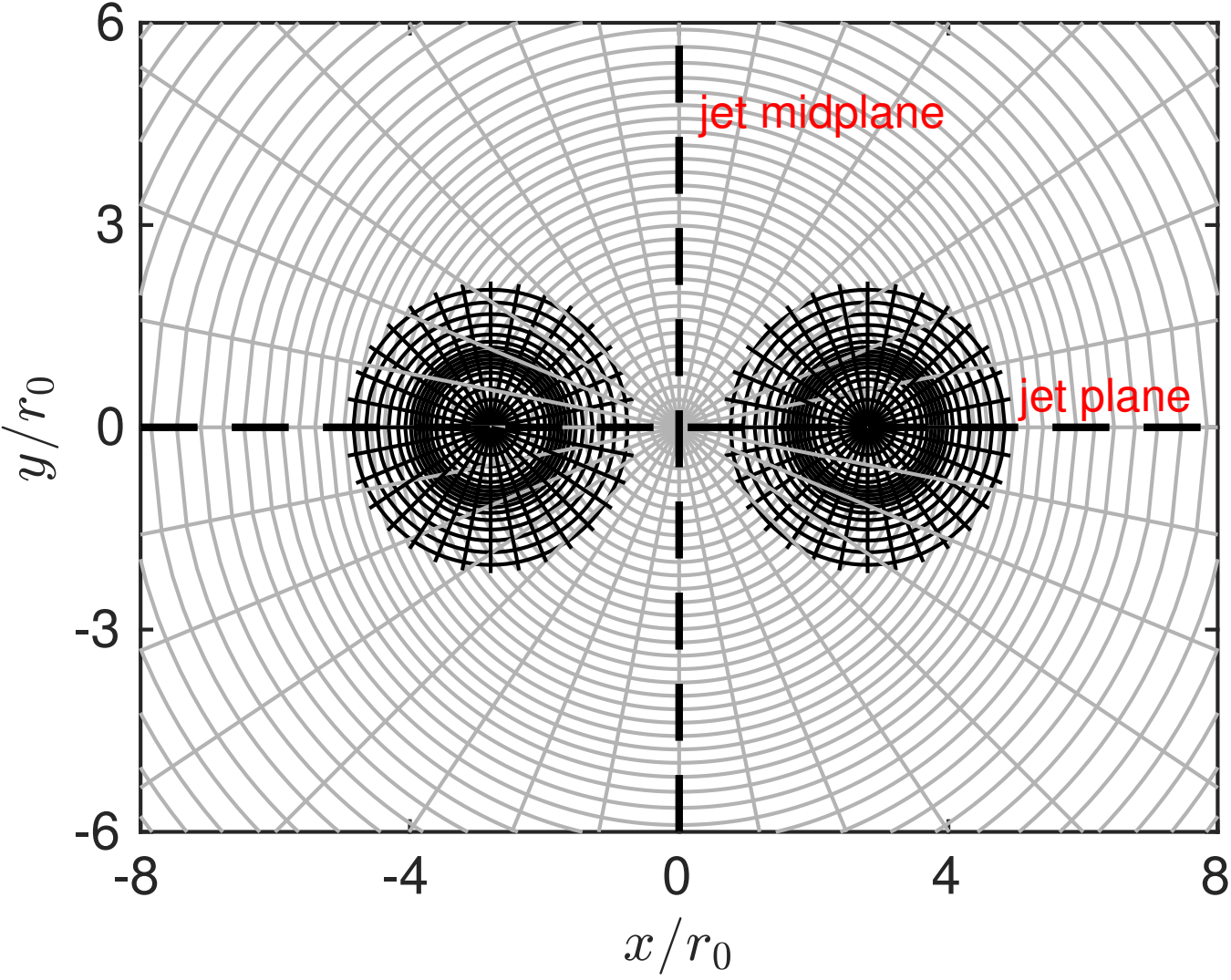
jet midplane
jet plane
6
3
0
-3
-6
-8
-4
0
4
8
y/r_0
x/r_0

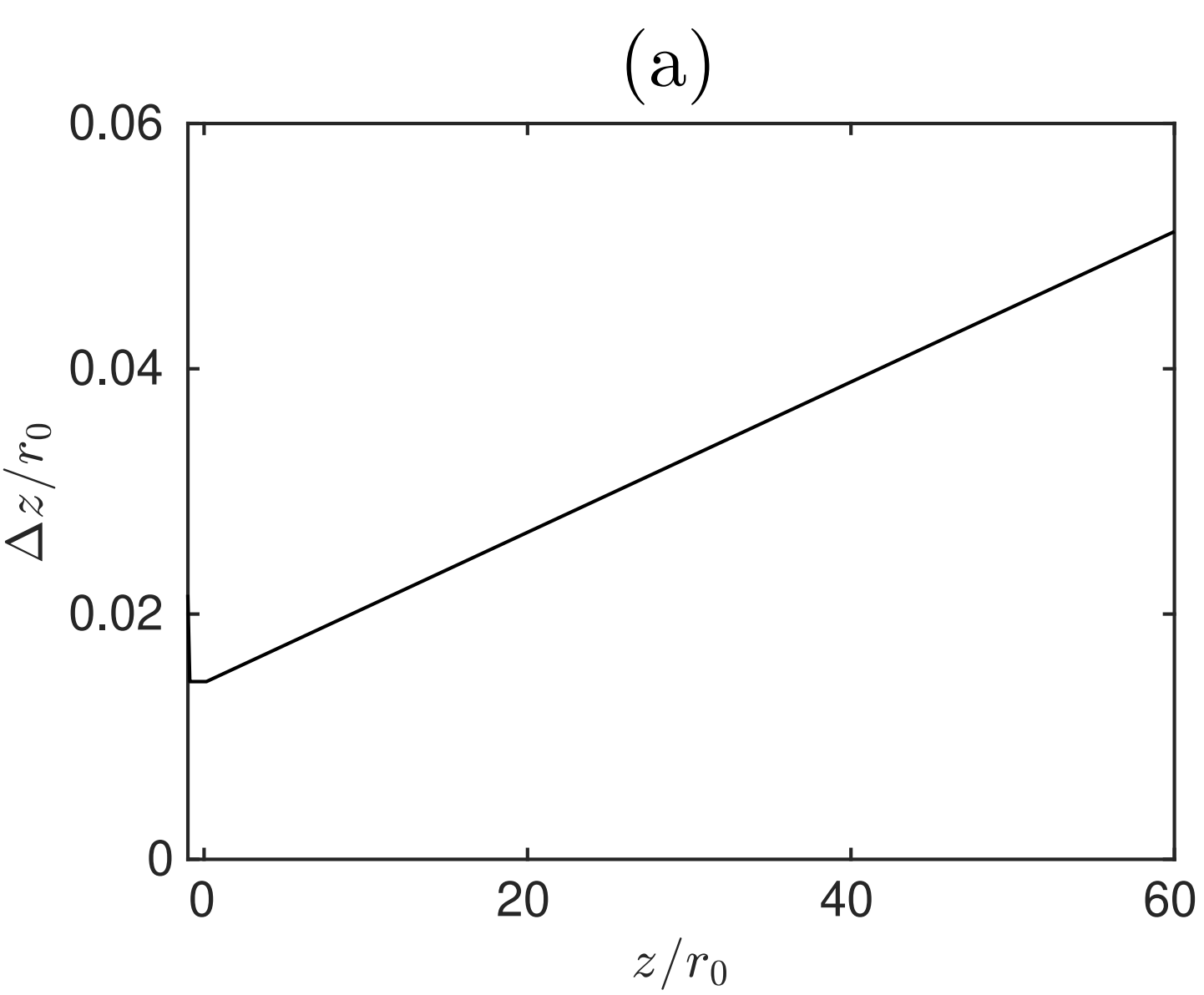
(a)
0.06
0.04
0.02
0
$\Delta z/r_0$
0
20
40
60
z/r_0

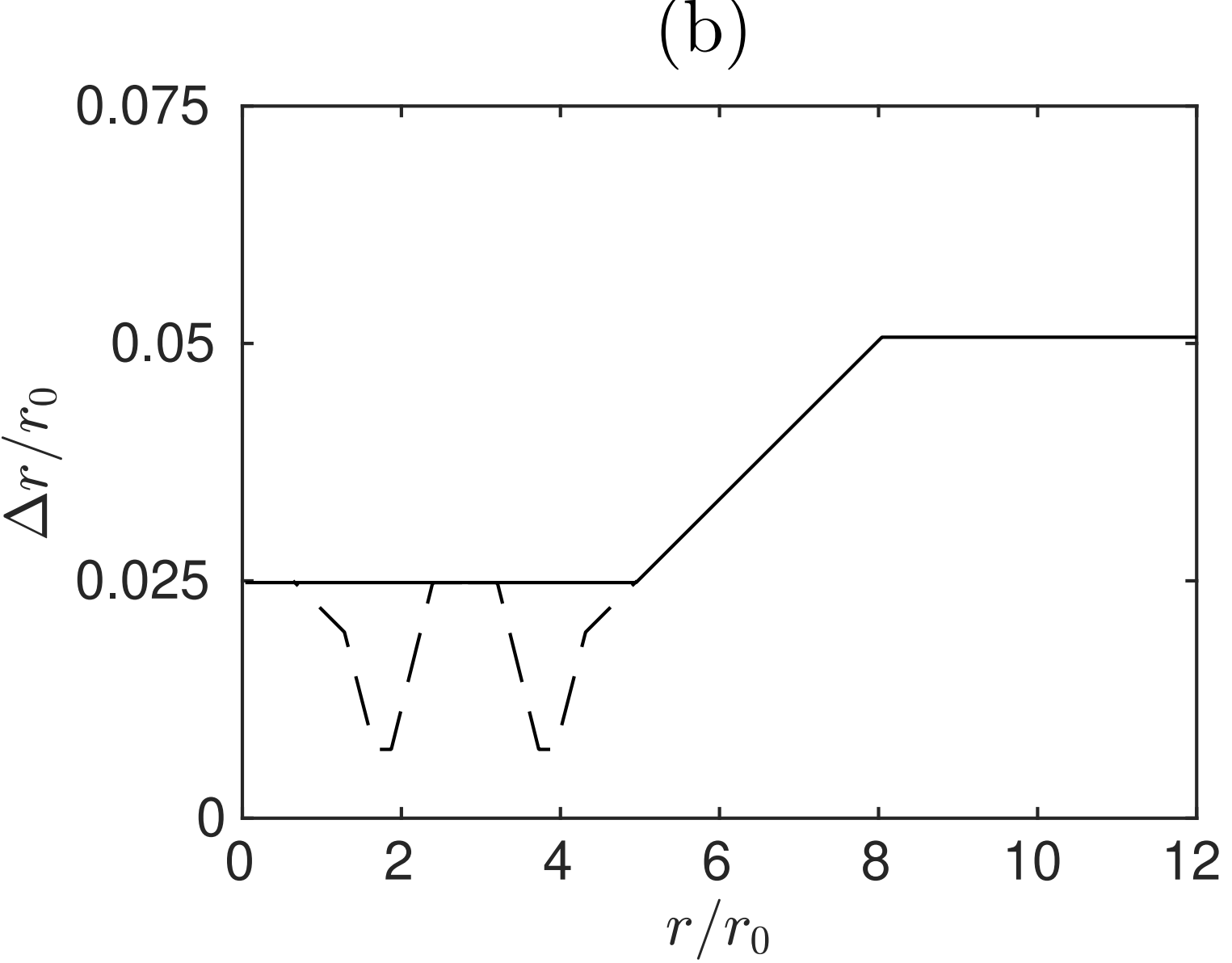
(b)
0.075
0.05
0.025
0
$\Delta r/r_0$
0
2
4
6
8
10
12
r/r_0

(a)

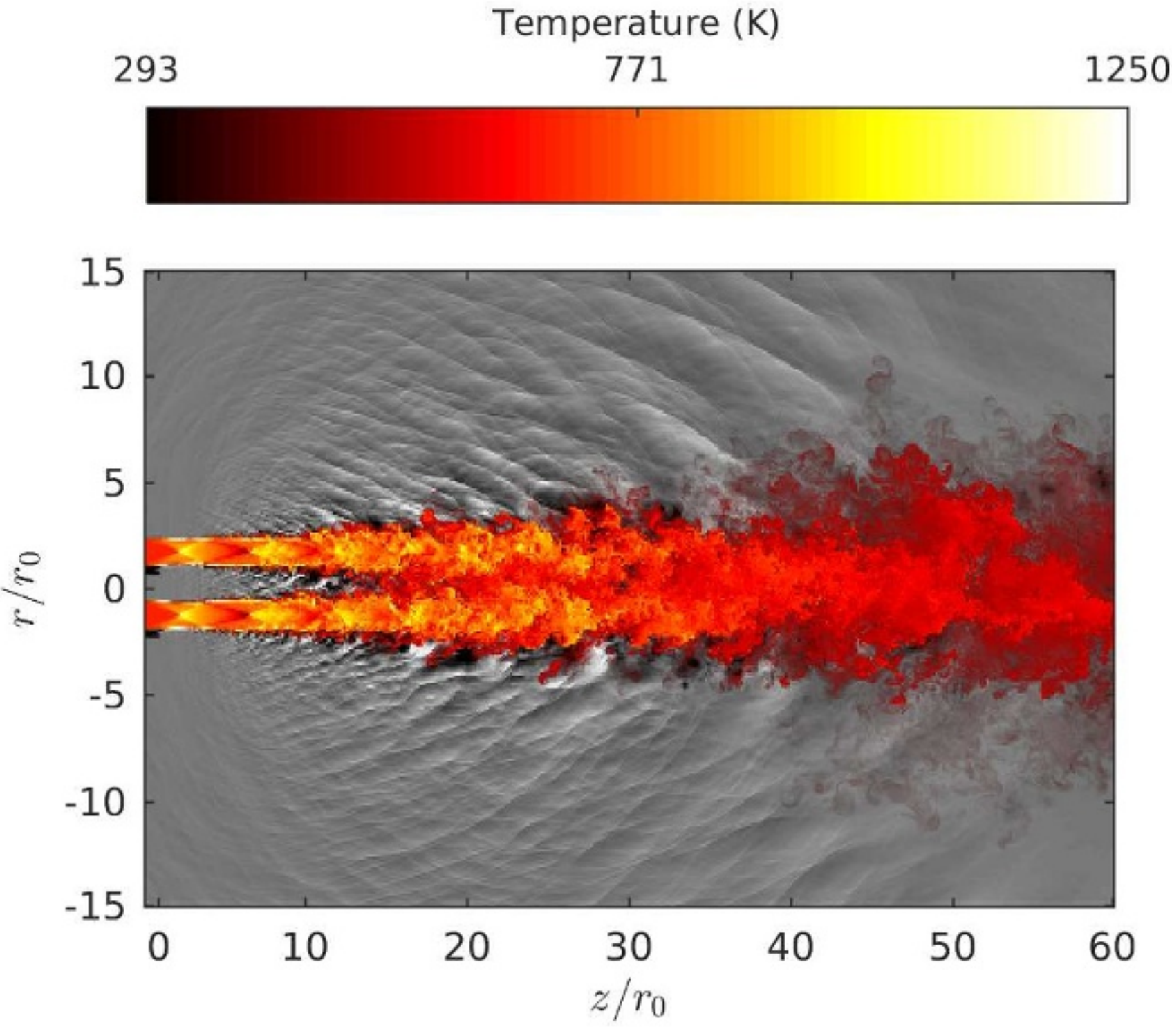
Temperature (K)
293
771
1250
15
10
5
0
-5
-10
-15
r/r_0
0
10
20
30
40
50
60
z/r_0

(b)

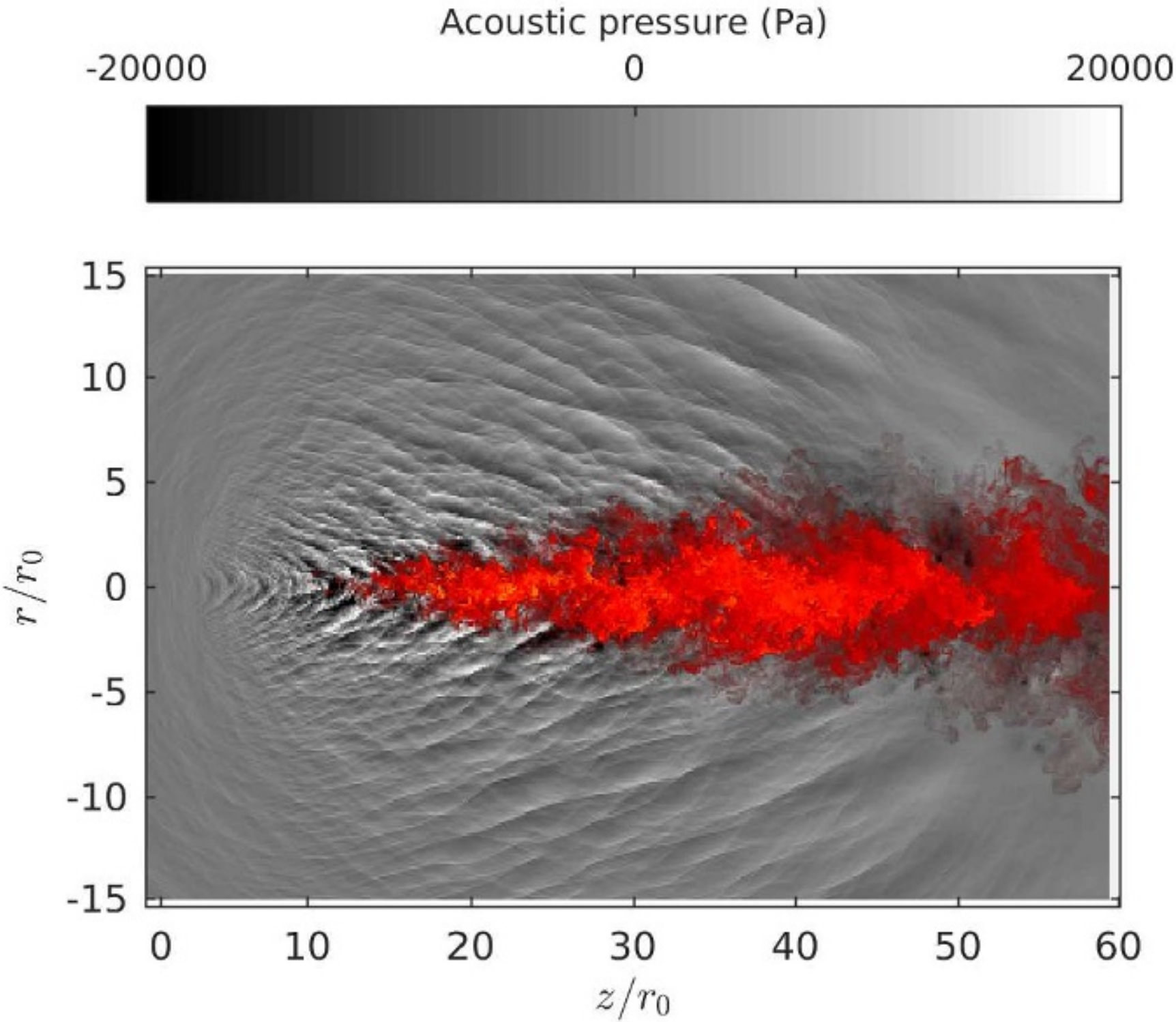
Acoustic pressure (Pa)
-20000
0
20000
15
10
5
0
-5
-10
-15
r/r_0
0
10
20
30
40
50
60
z/r_0

(c)

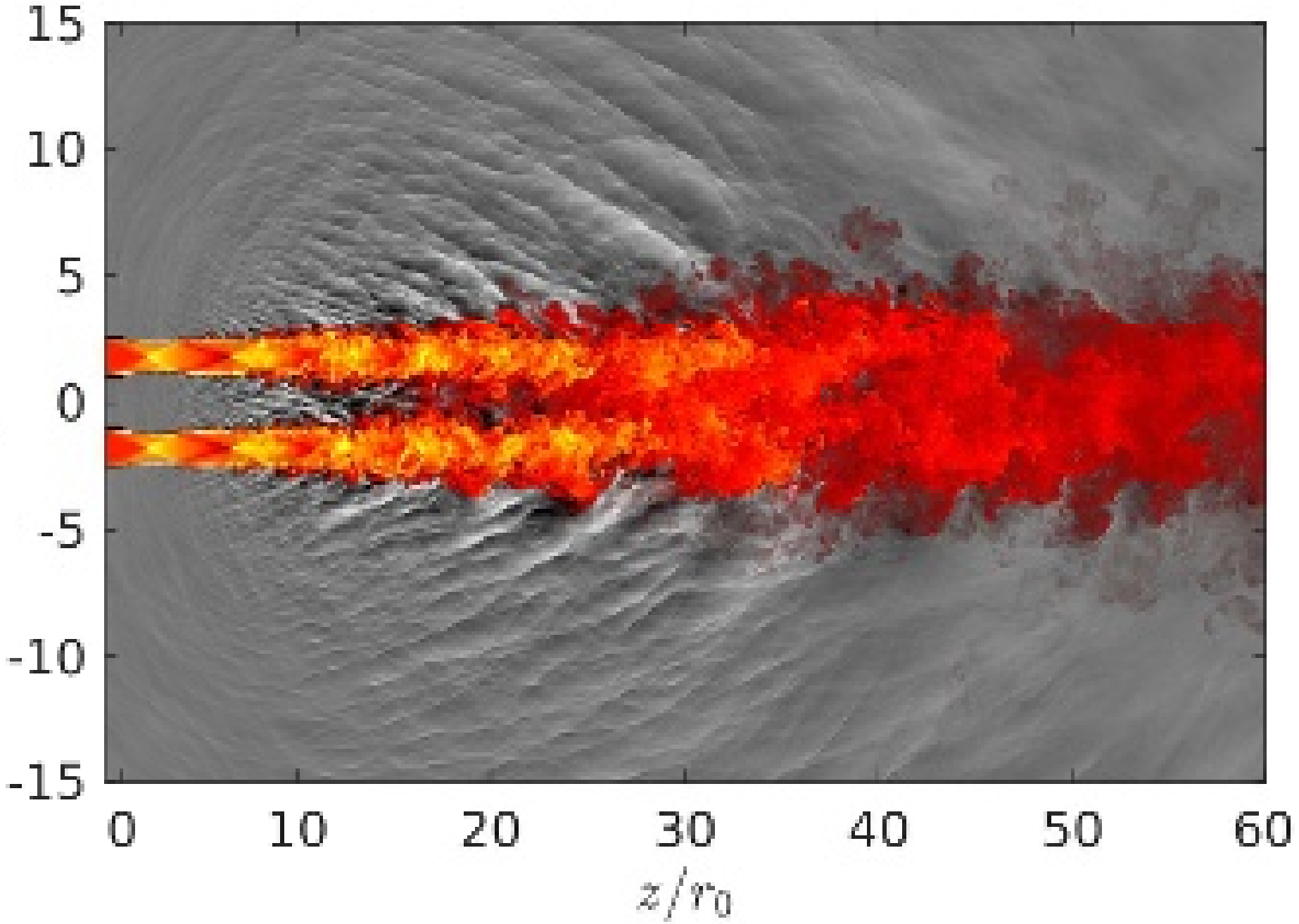

(d)

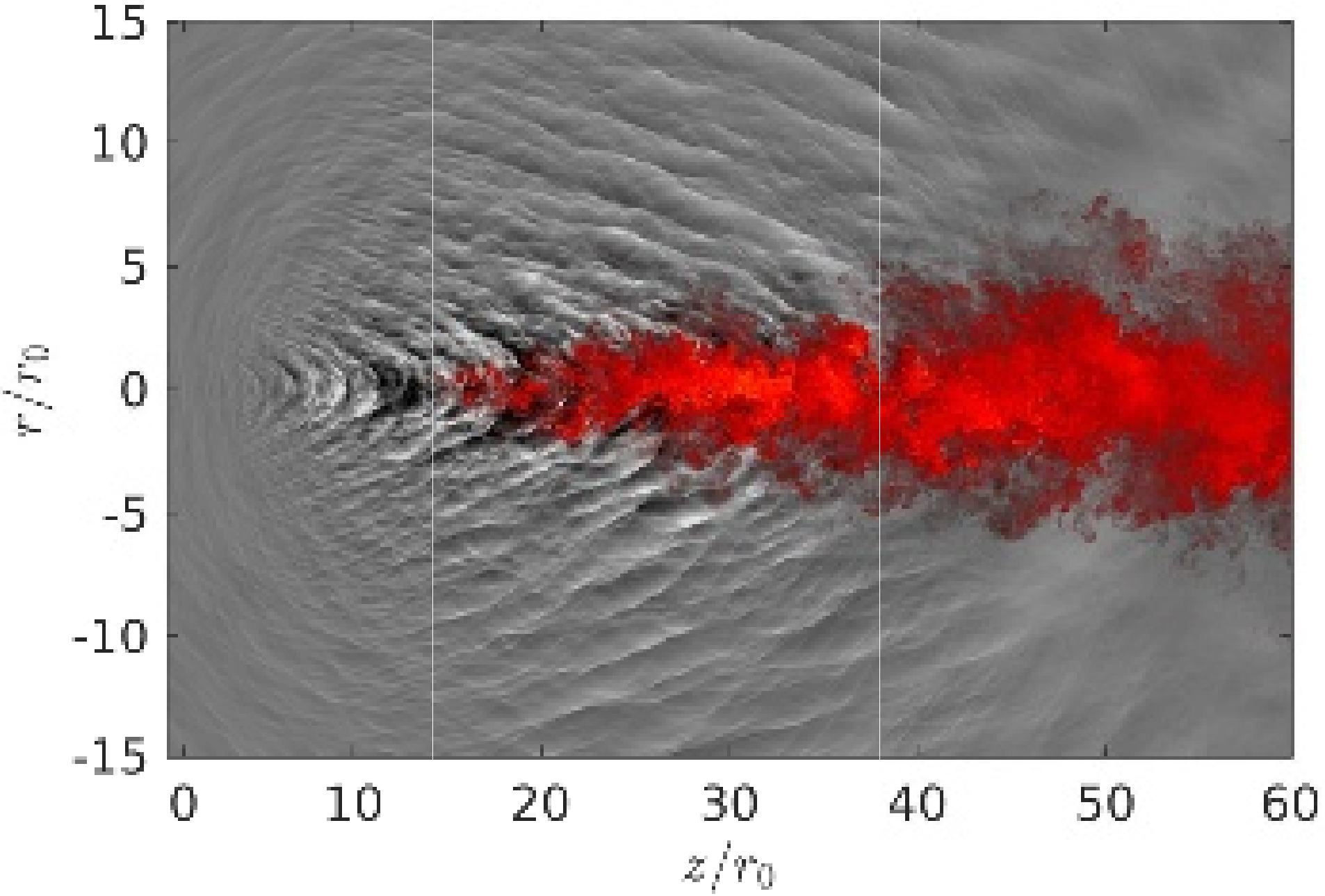

(e)

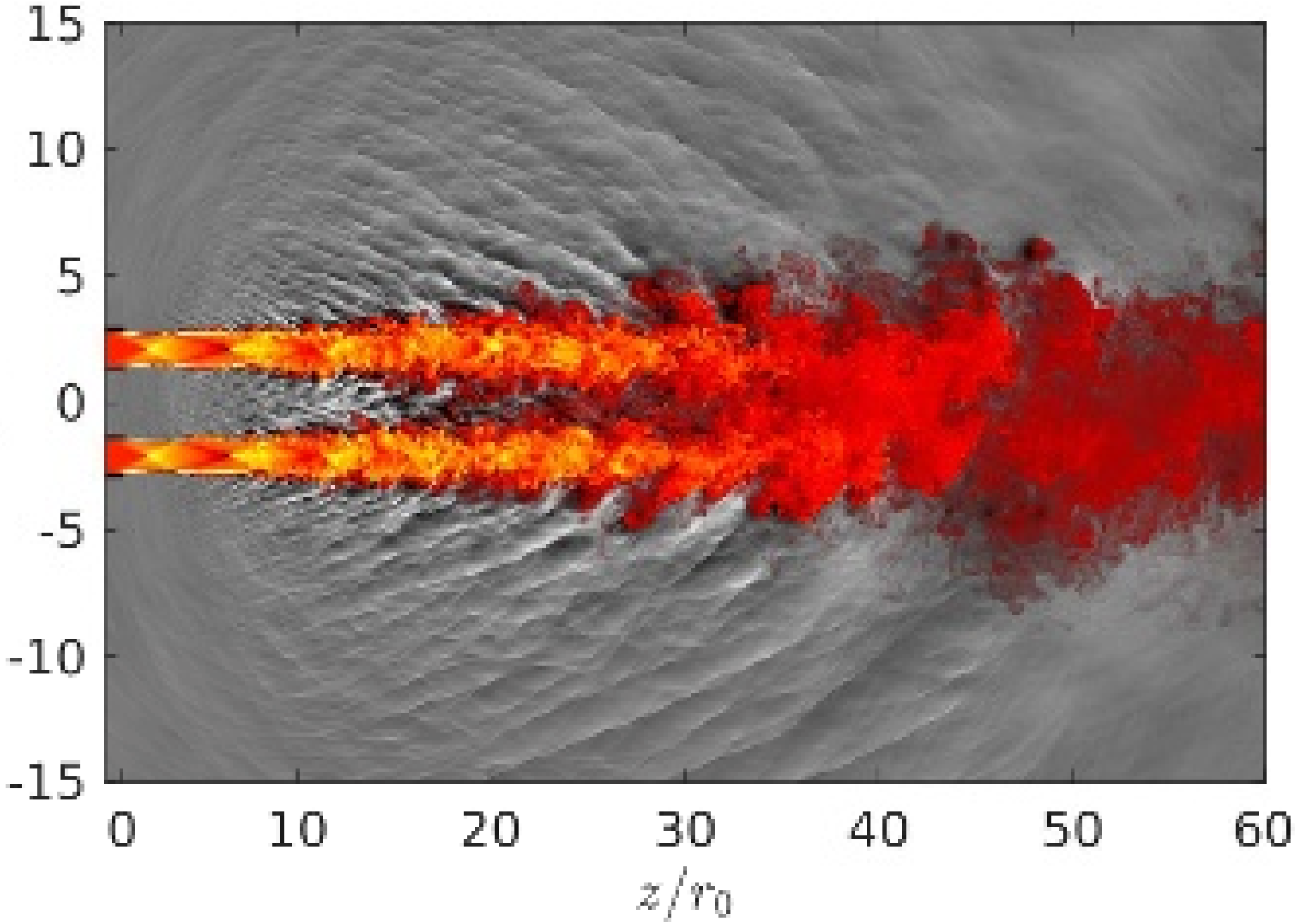

(f)

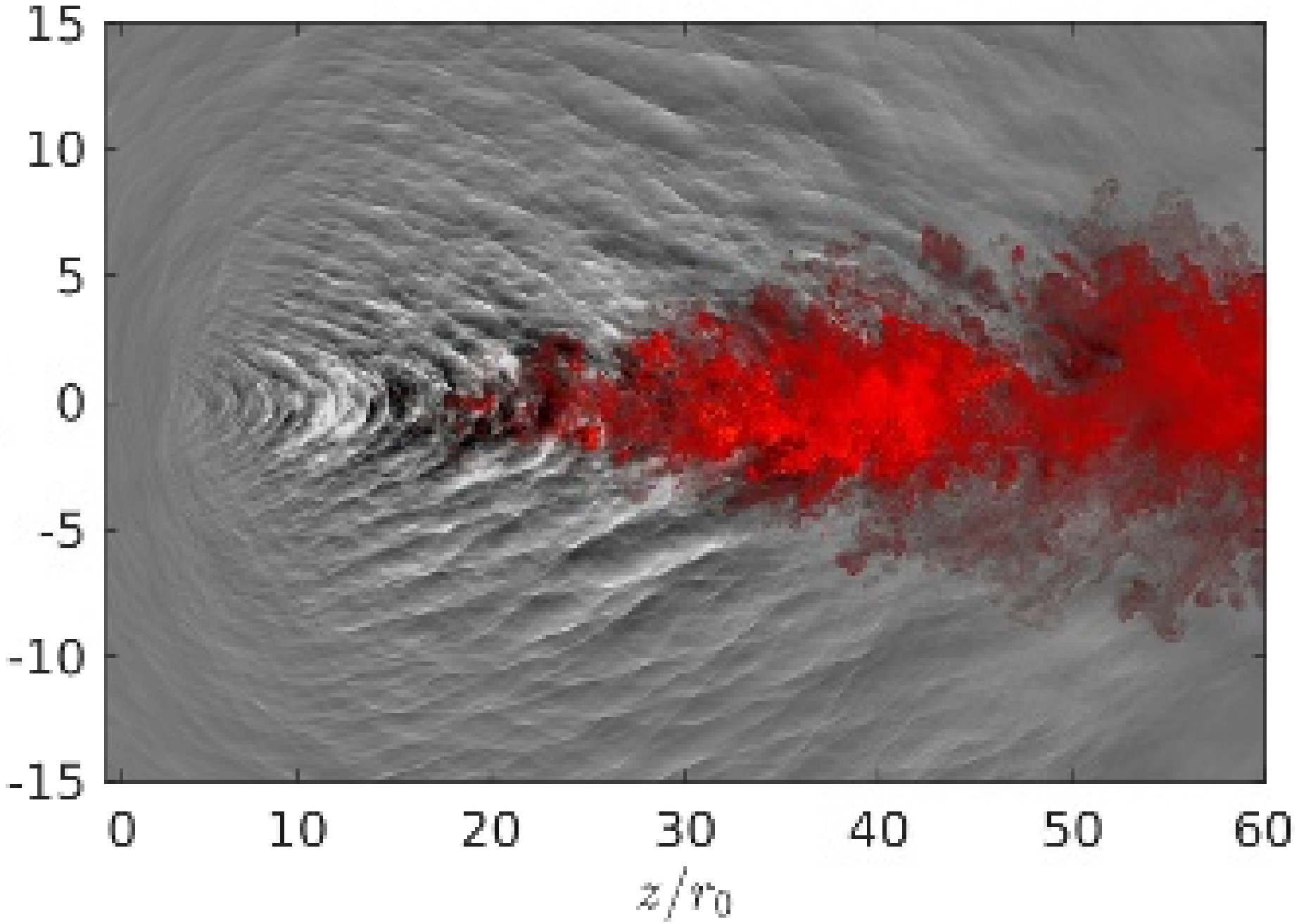

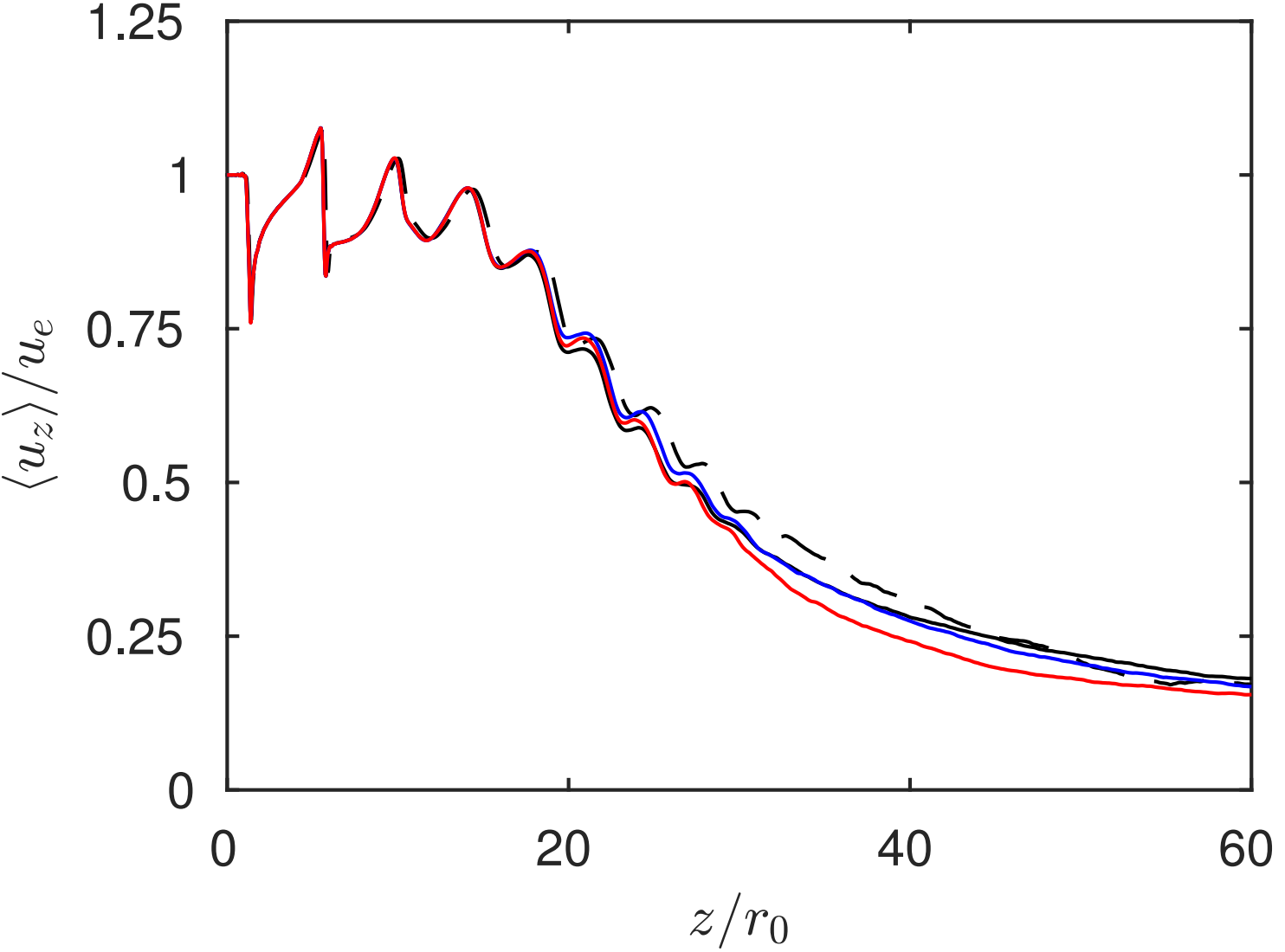
1.25
1
0.75
0.5
0.25
0
0
20
40
60
$\langle u_z \rangle / u_e$
z/r_0

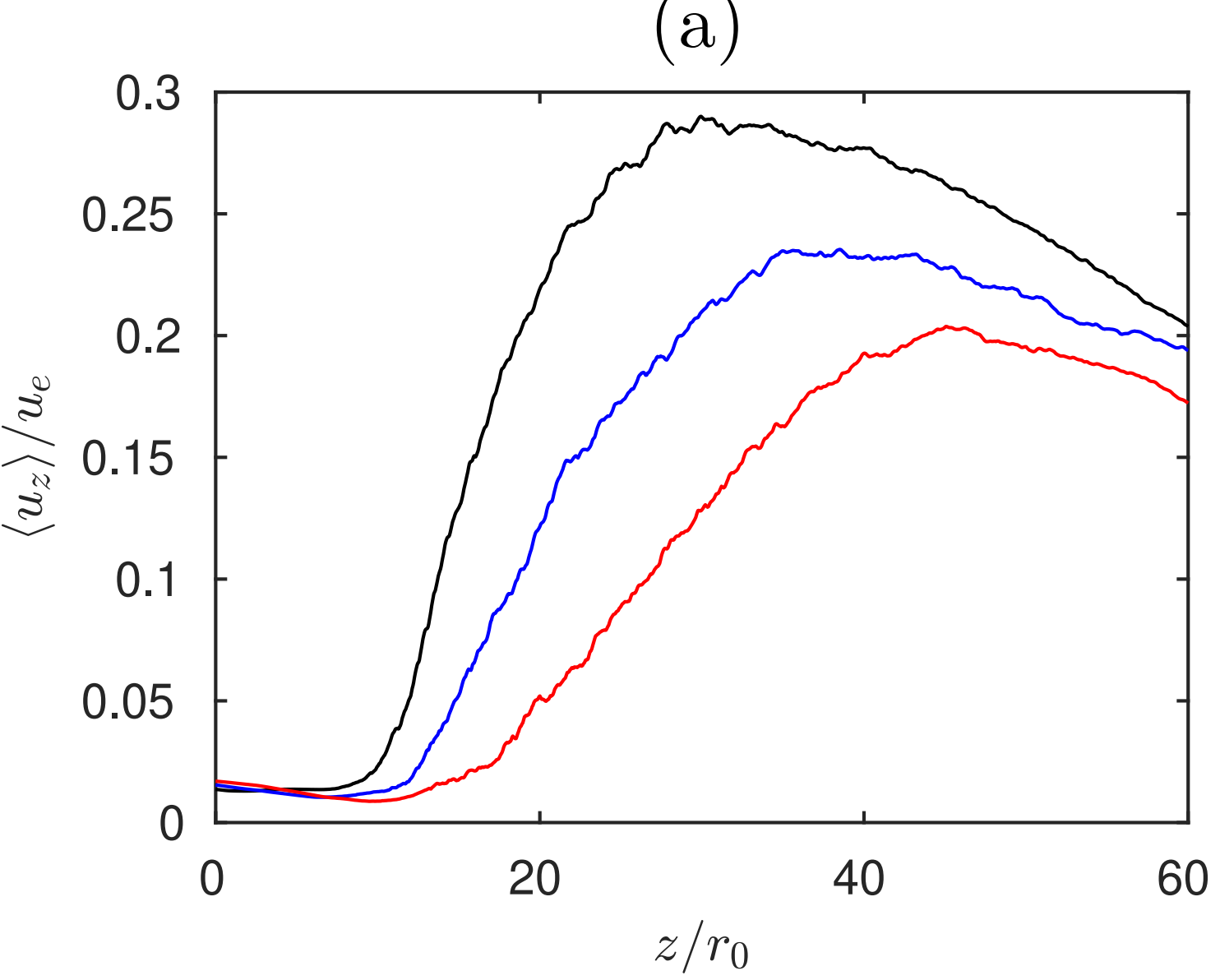
(a)
0.3
0.25
0.2
0.15
0.1
0.05
0
$\langle u_z \rangle / u_e$
0
20
40
60
z/r_0

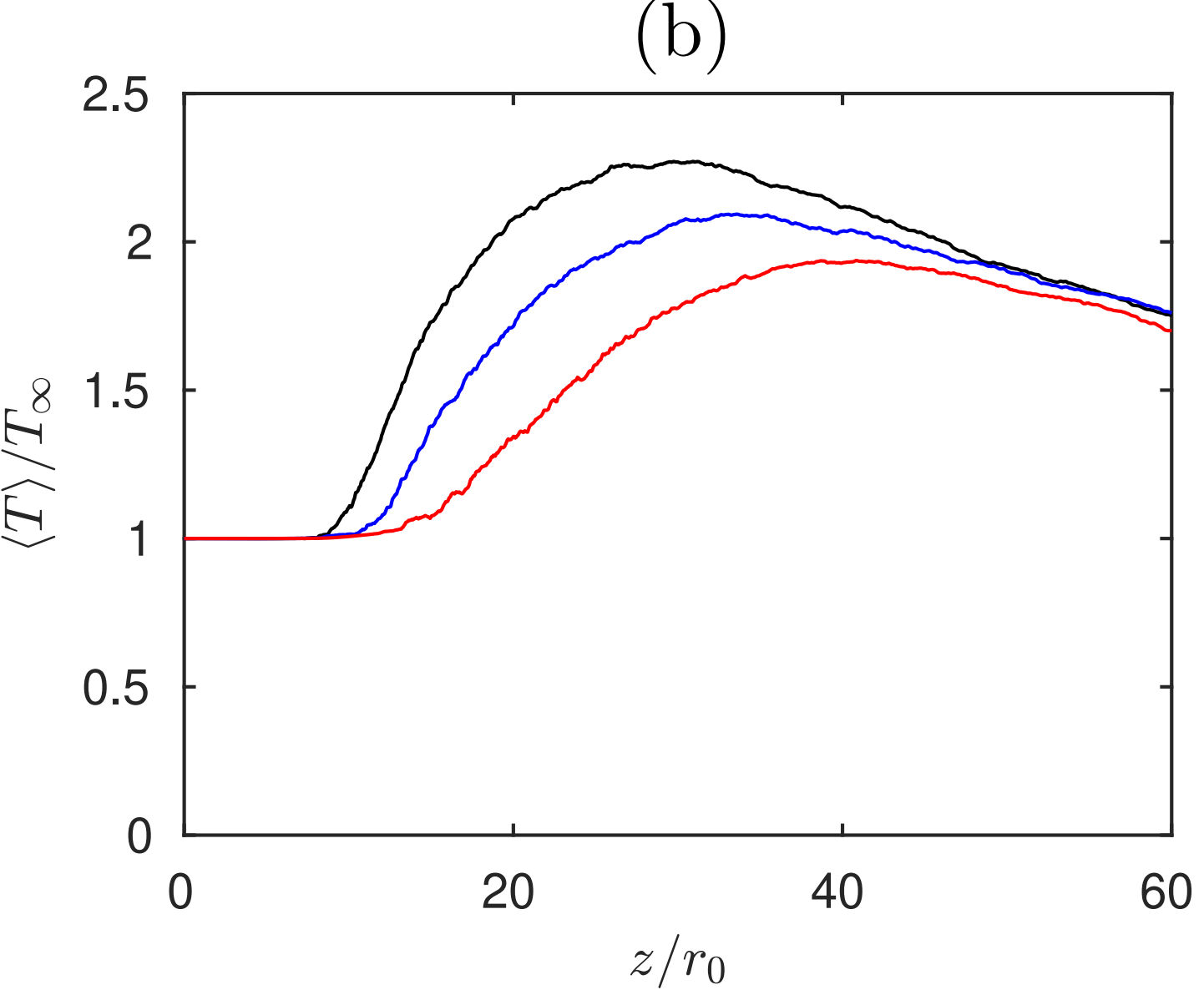
(b)
2.5
2
1.5
1
0.5
0
0
20
40
60
$\langle T \rangle / T_\infty$
z/r_0

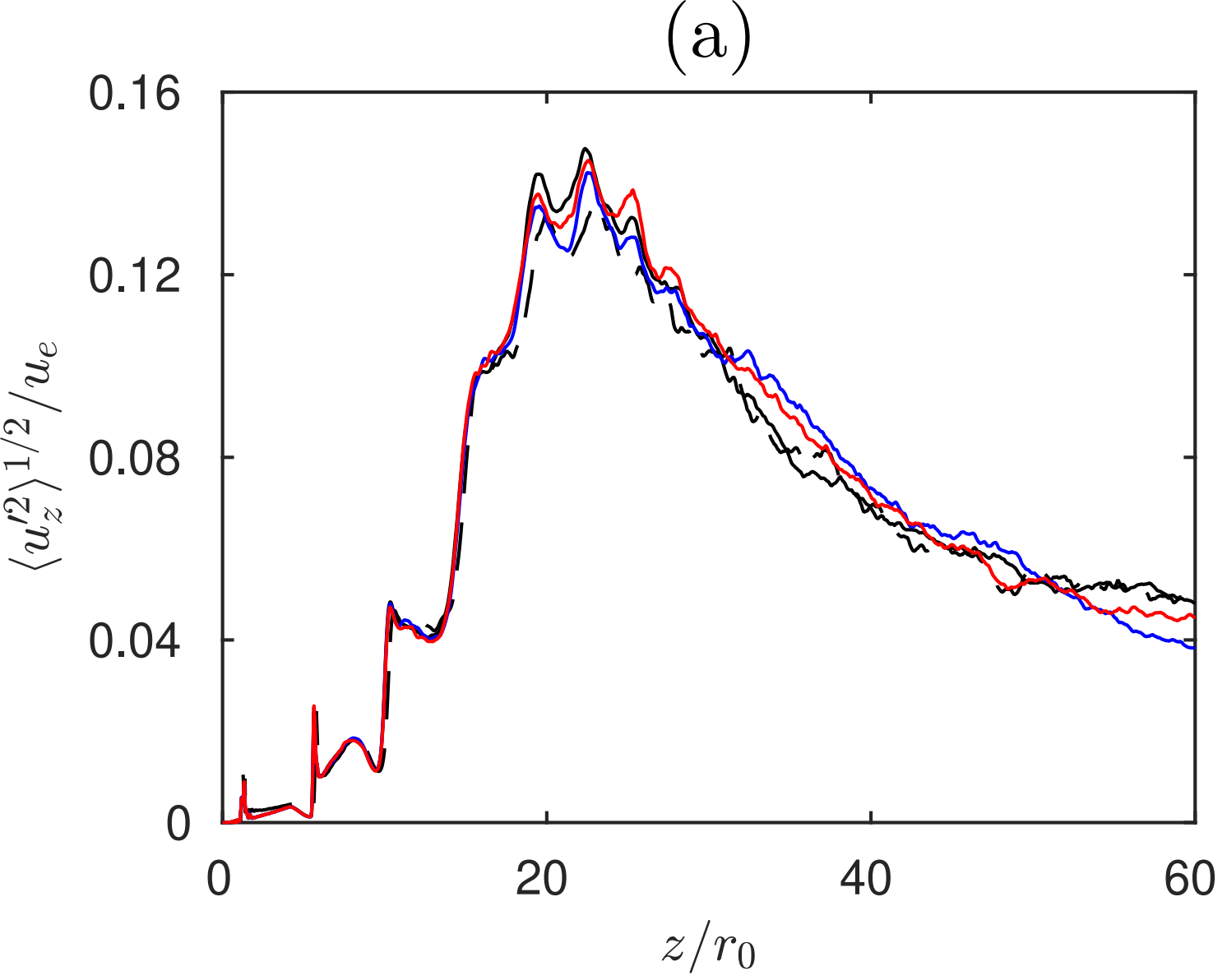
(a)
0.16
0.12
0.08
0.04
0
$\langle u_z'^2 \rangle^{1/2}/u_e$
0
20
40
60
z/r_0

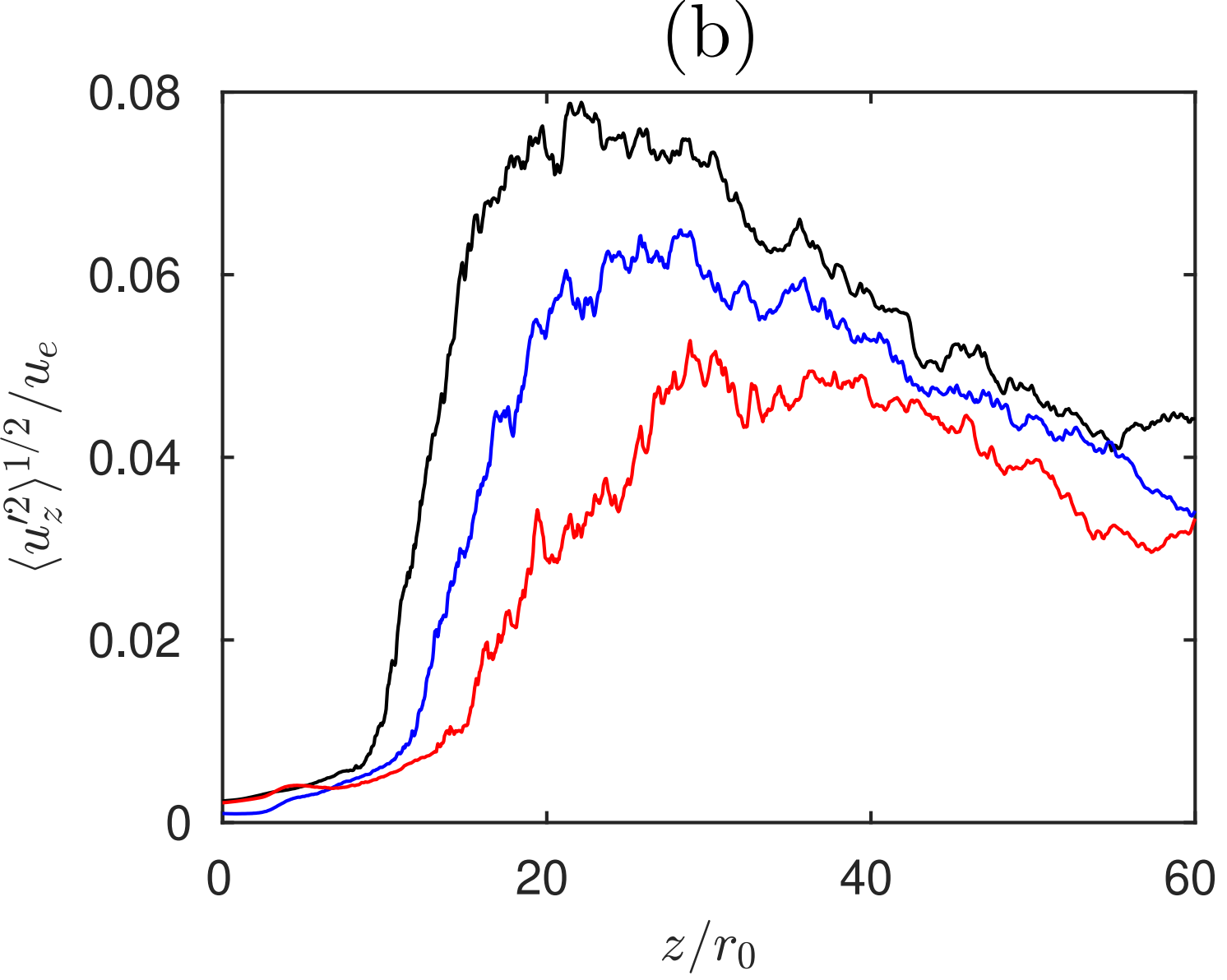
(b)
0.08
0.06
0.04
0.02
0
$\langle u_z'^2 \rangle^{1/2}/u_e$
0
20
40
60
z/r_0

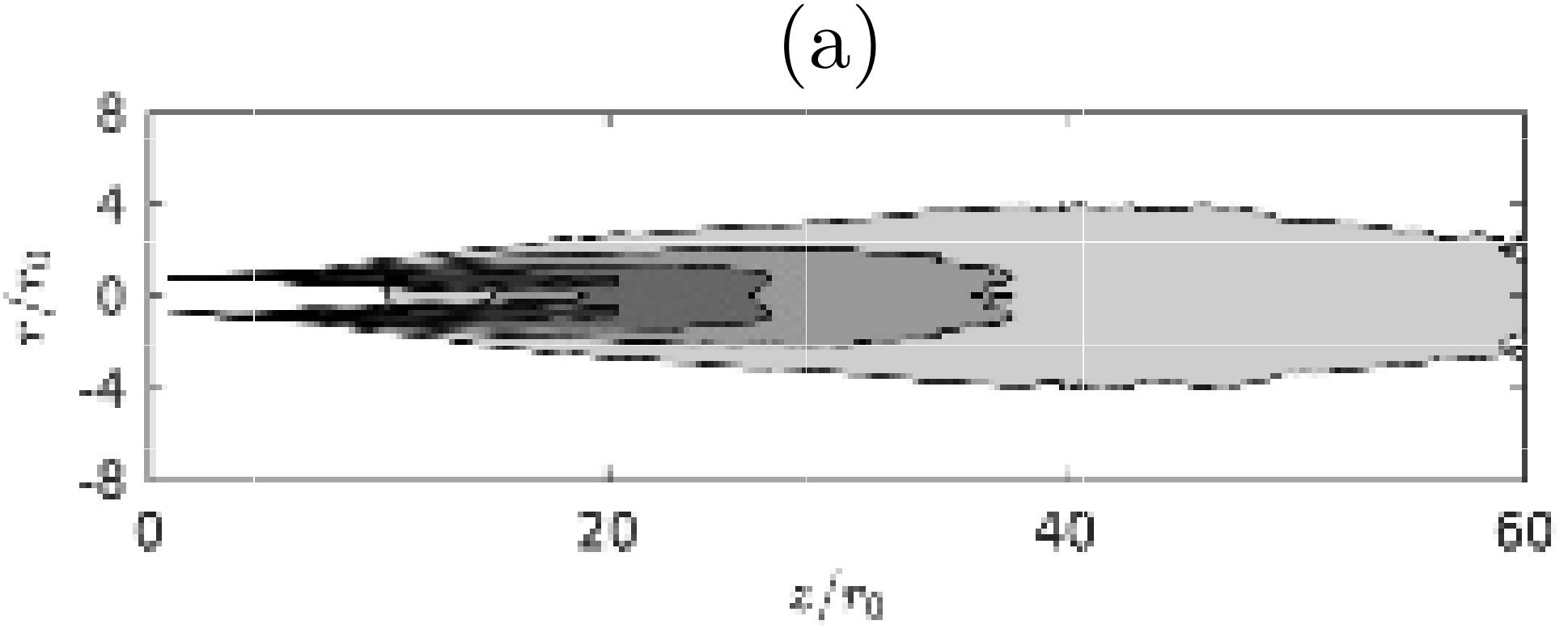
(a)
8
4
0
-4
-8
r/r0
0
20
40
60
x/r0

(b)

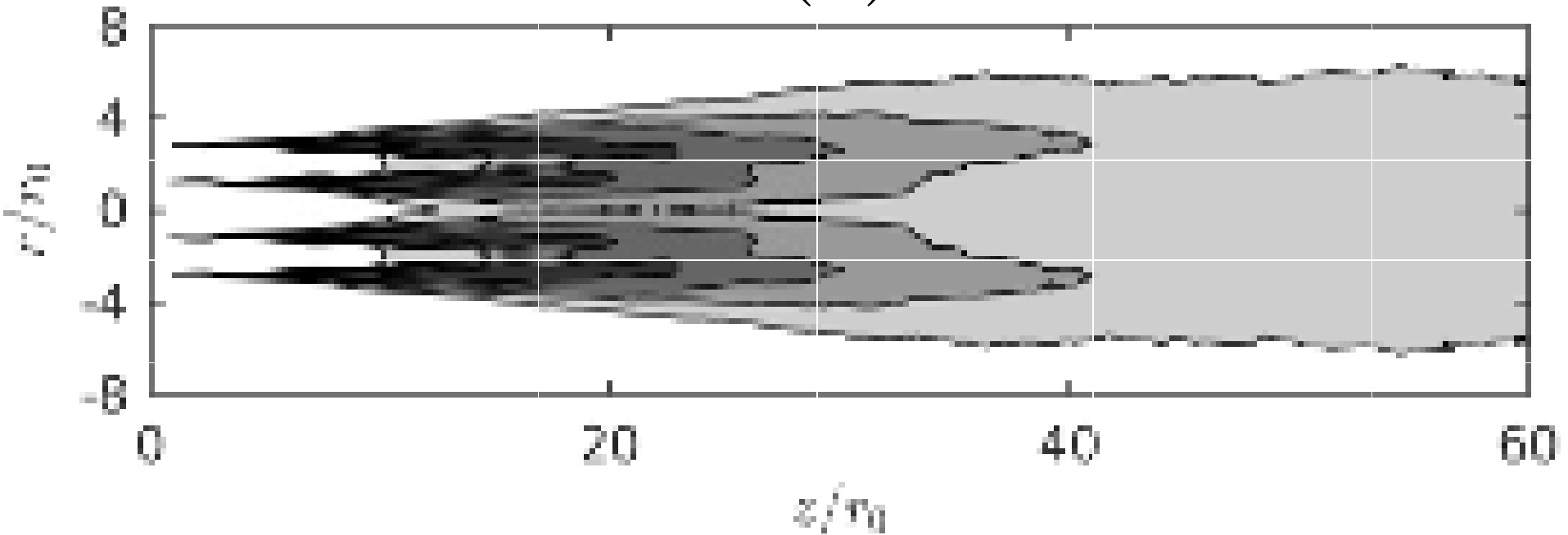

(c)

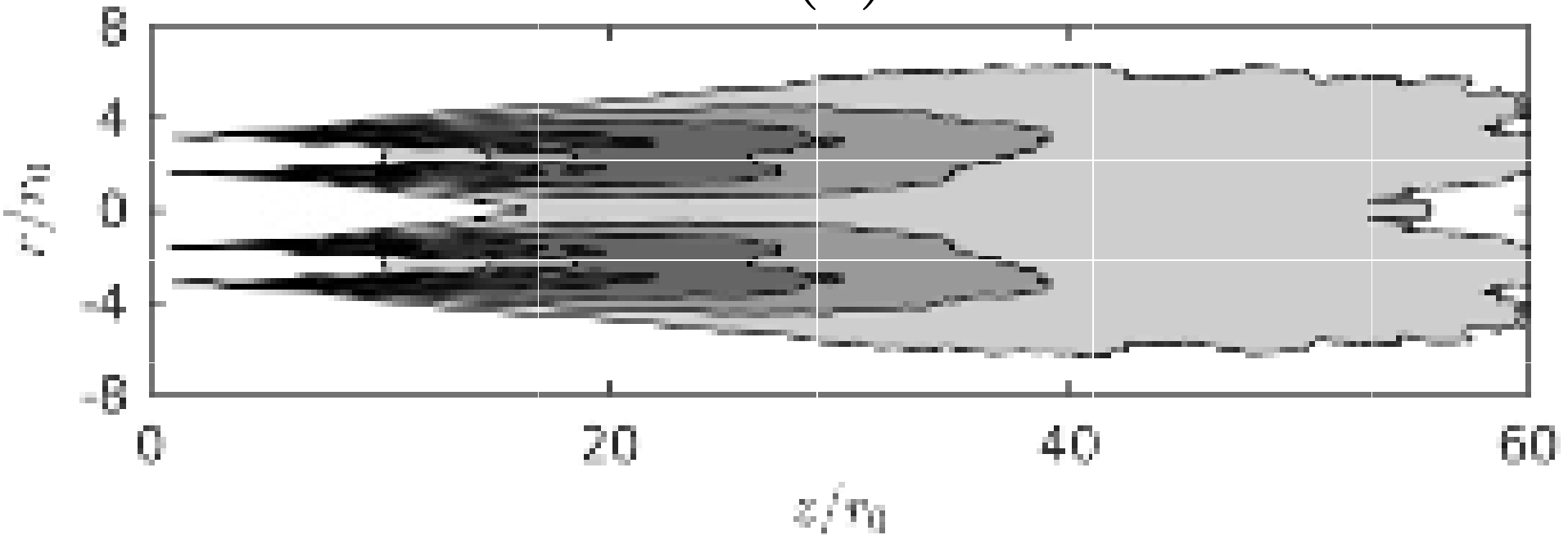

(d)

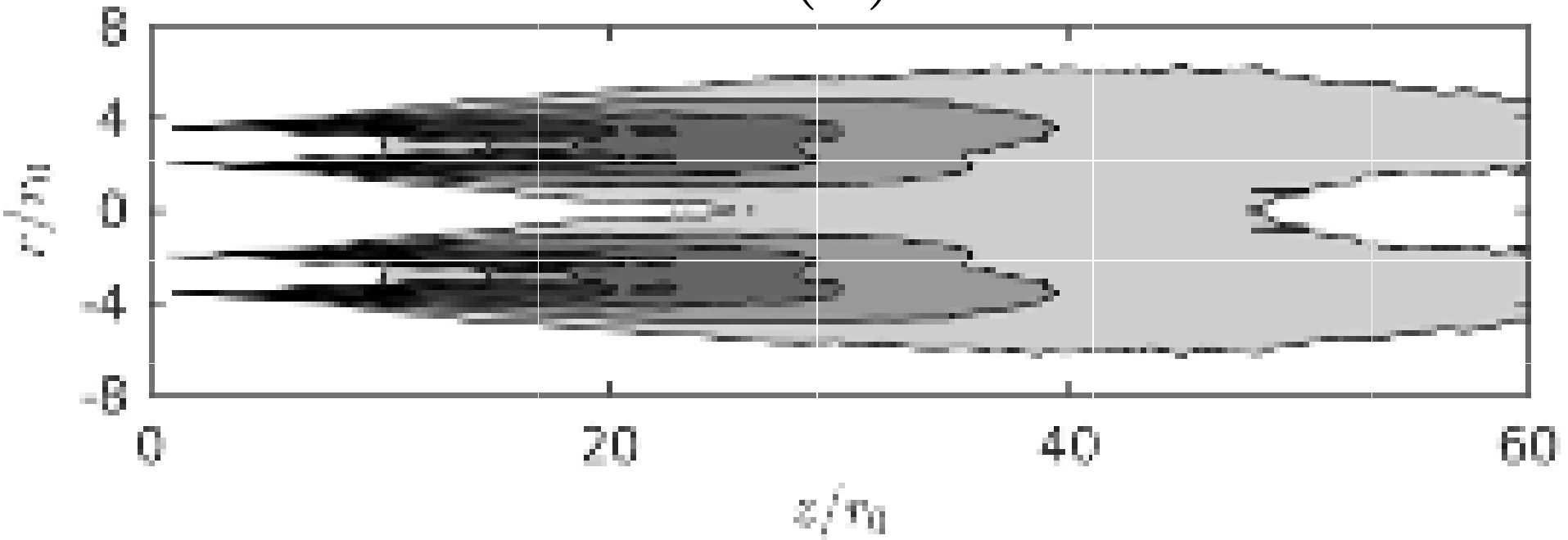

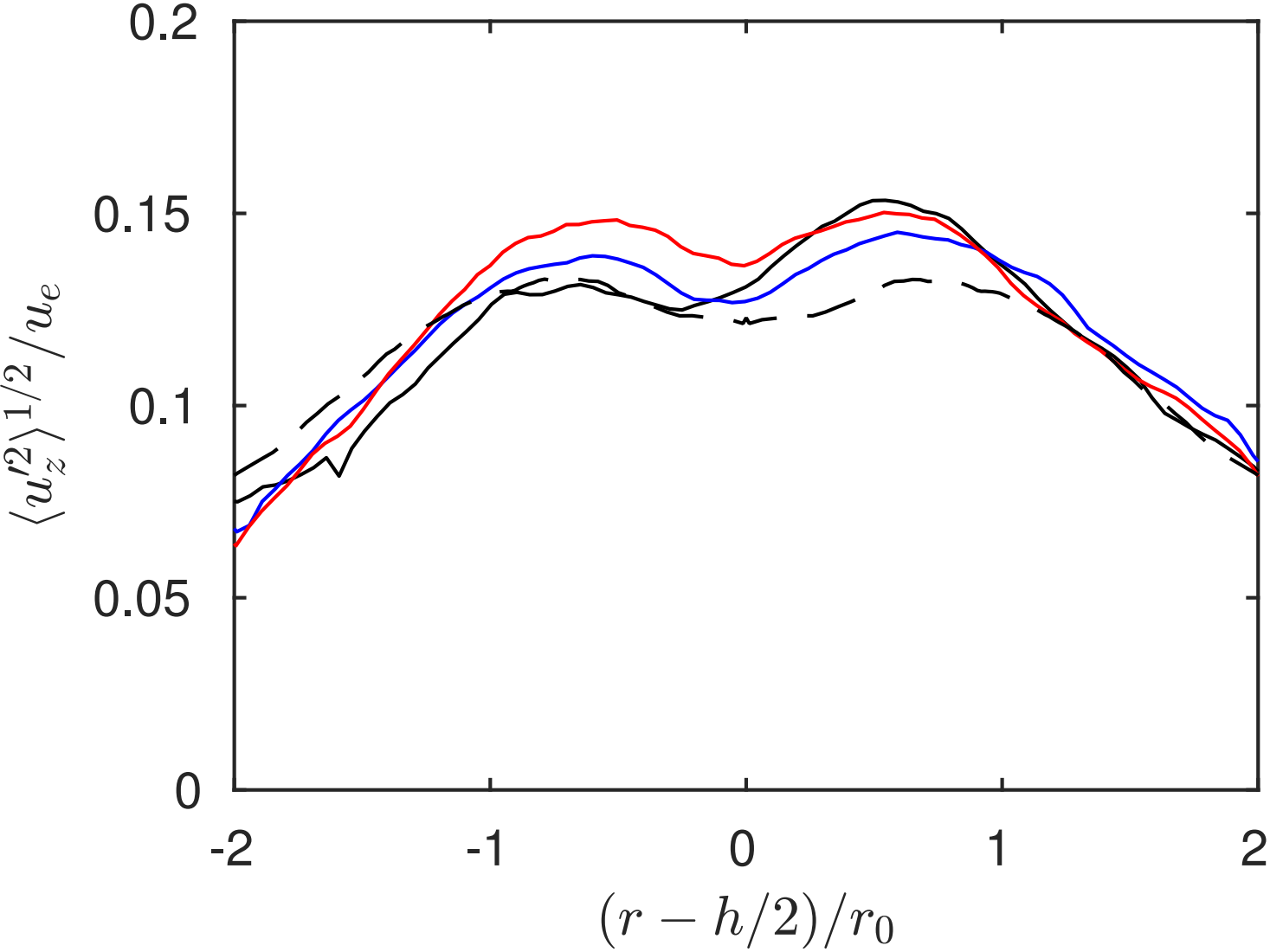
0.2
0.15
0.1
0.05
0
-2
-1
0
1
2
$\langle u_z'^2 \rangle^{1/2}/u_e$
$(r - h/2)/r_0$

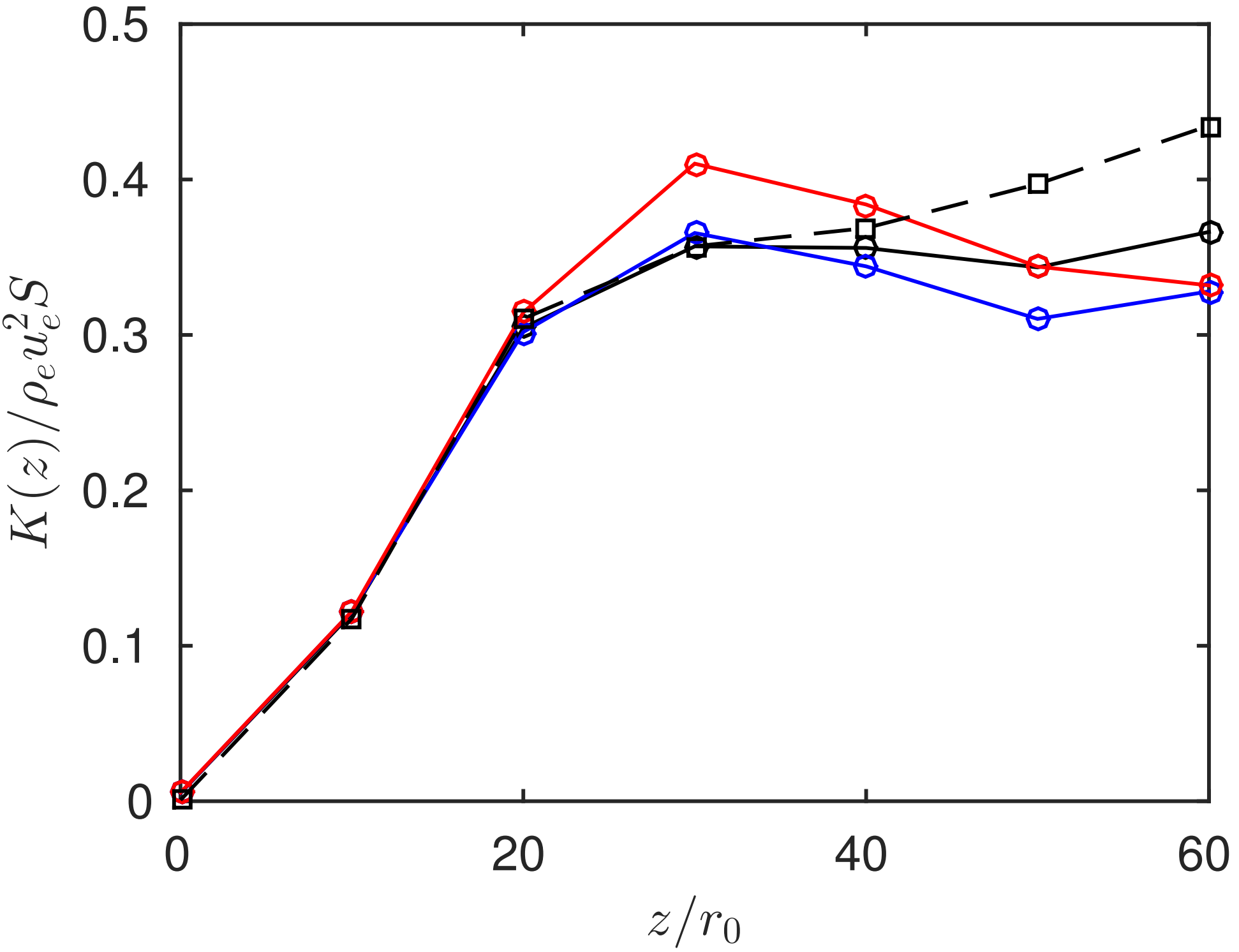
0.5
0.4
0.3
0.2
0.1
0
0
20
40
60
$K(z)/\rho_e u_e^2 S$
z/r_0

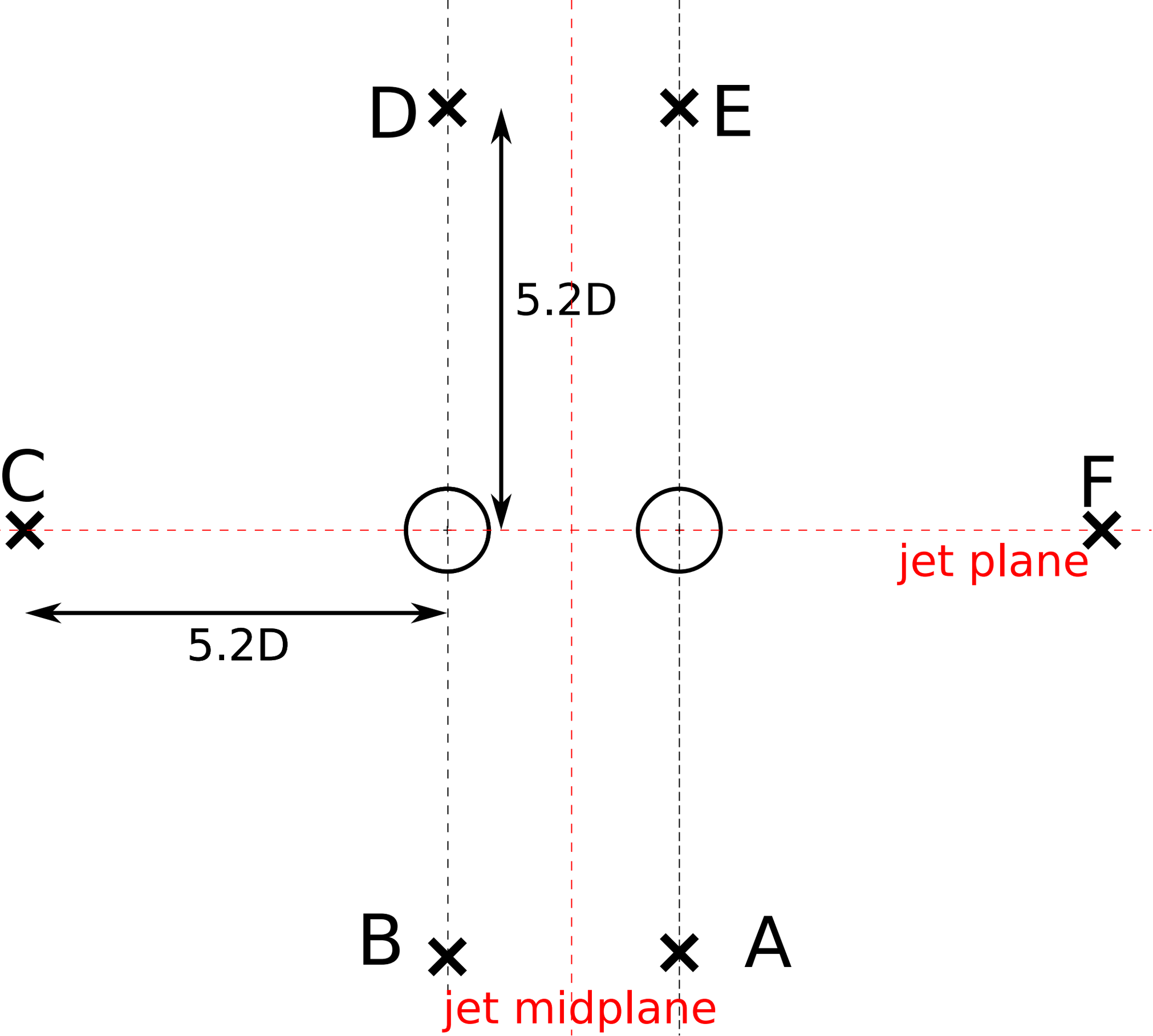
D
E
5.2D
C
F
jet plane
5.2D
B
A
jet midplane

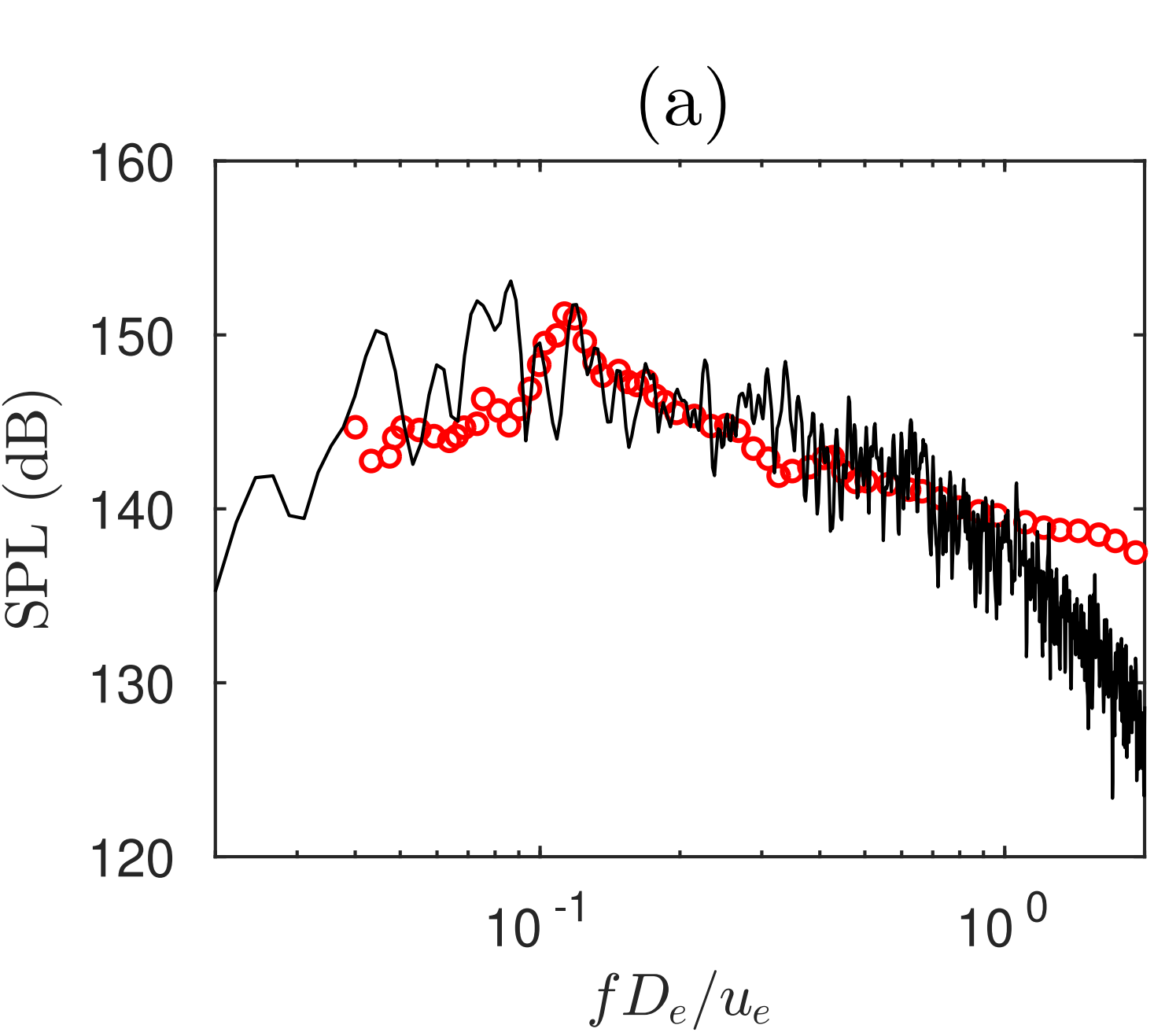
(a)
160
150
140
130
120
SPL (dB)
10^{-1}
10^{0}
fD_e/u_e

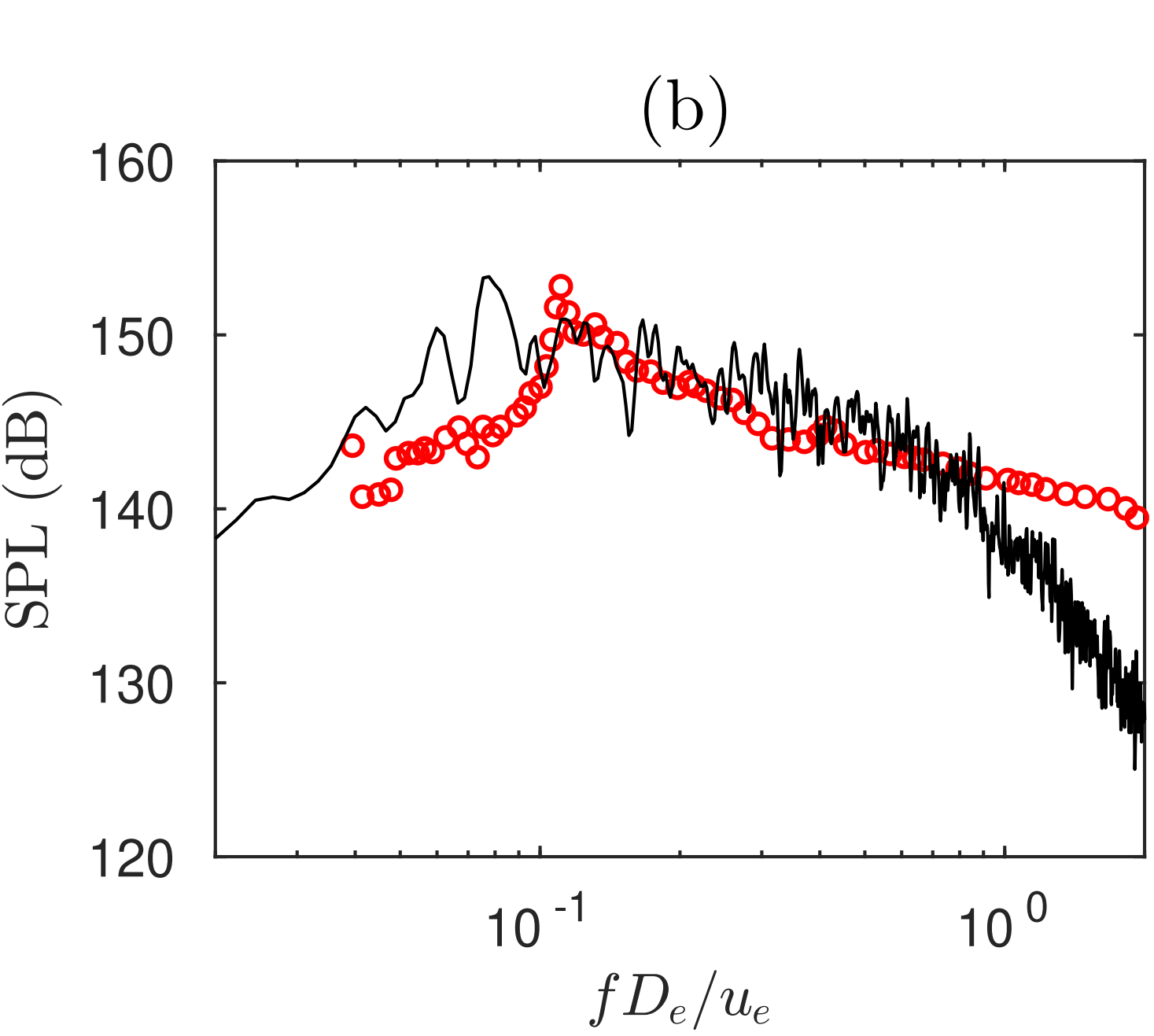
(b)
160
150
140
130
120
SPL (dB)
10^{-1}
10^{0}
fD_e/u_e

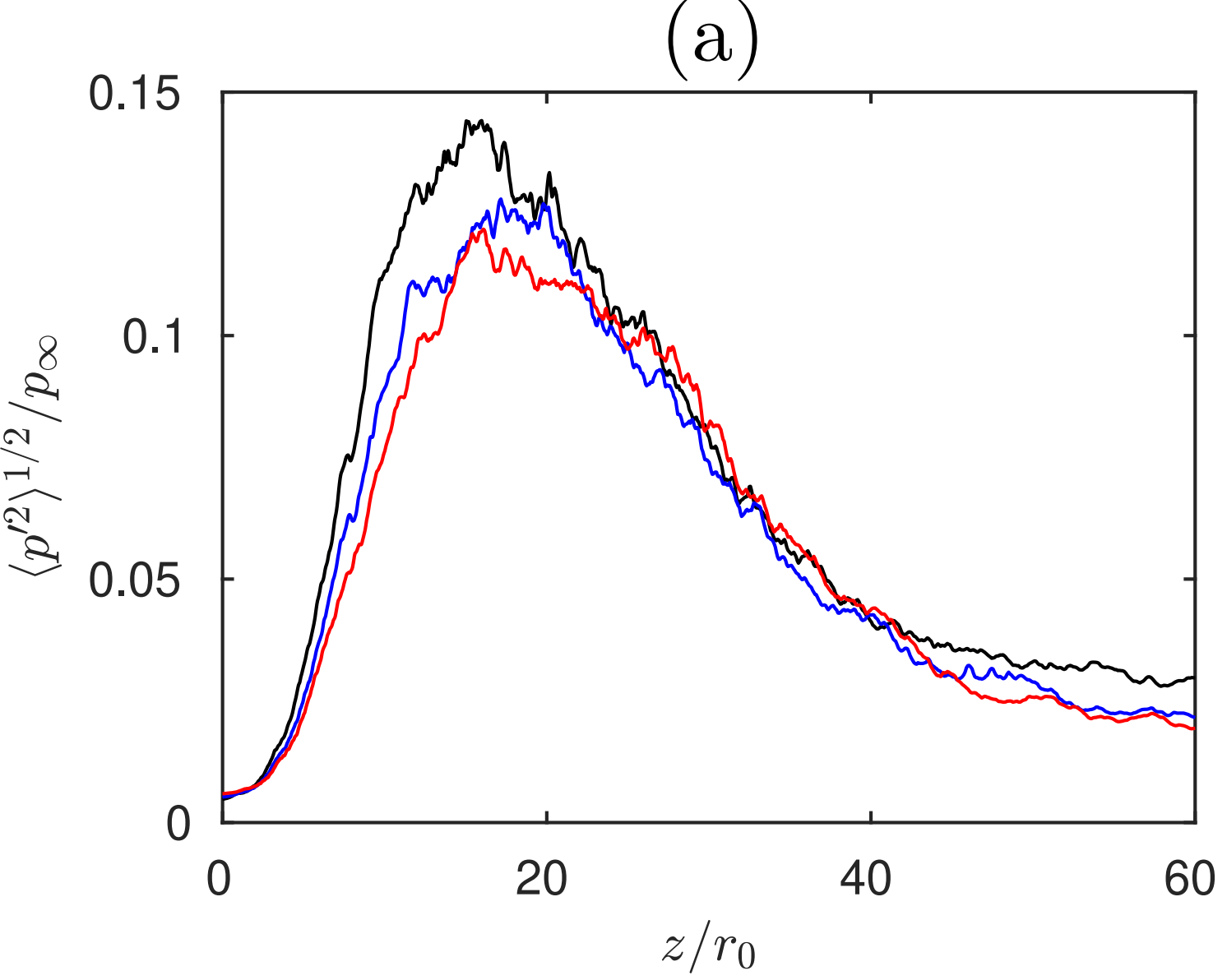
(a)
0.15
0.1
0.05
0
0
20
40
60
$\langle p'^2 \rangle^{1/2}/p_\infty$
z/r_0

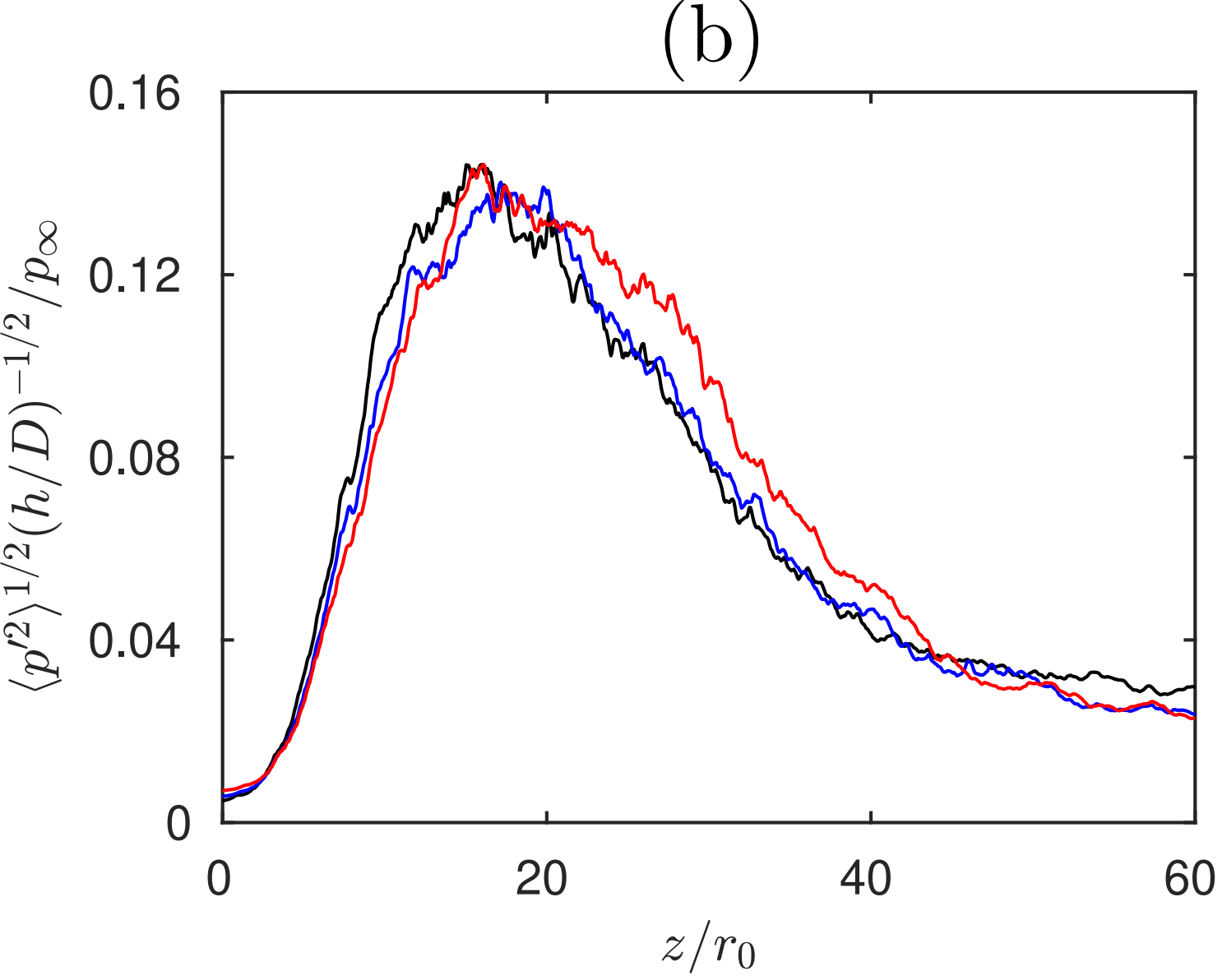
(b)
0.16
0.12
0.08
0.04
0
$\langle p'^2\rangle^{1/2}(h/D)^{-1/2}/p_\infty$
0
20
40
60
z/r_0

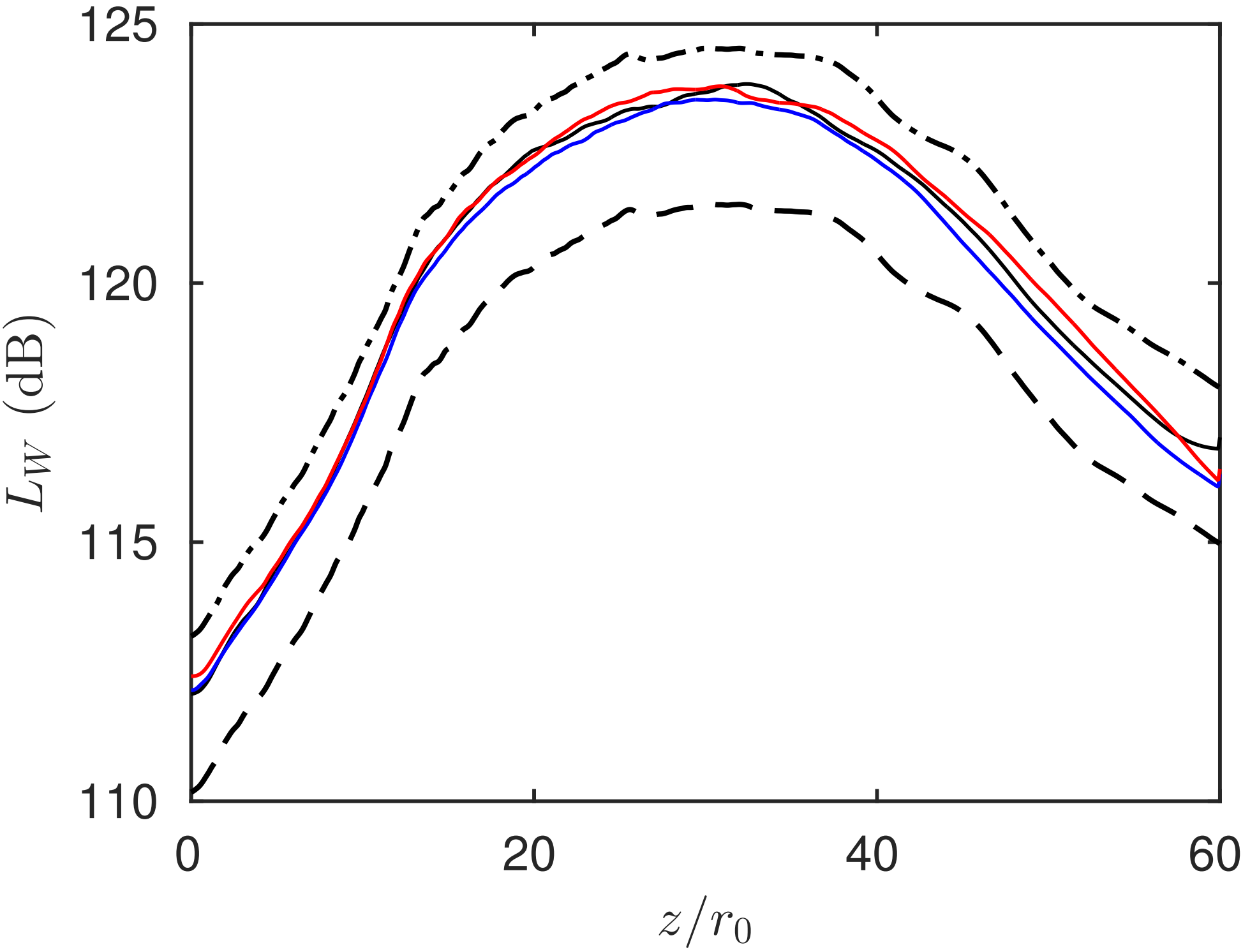
125
120
115
110
L_W (dB)
0
20
40
60
z/r_0

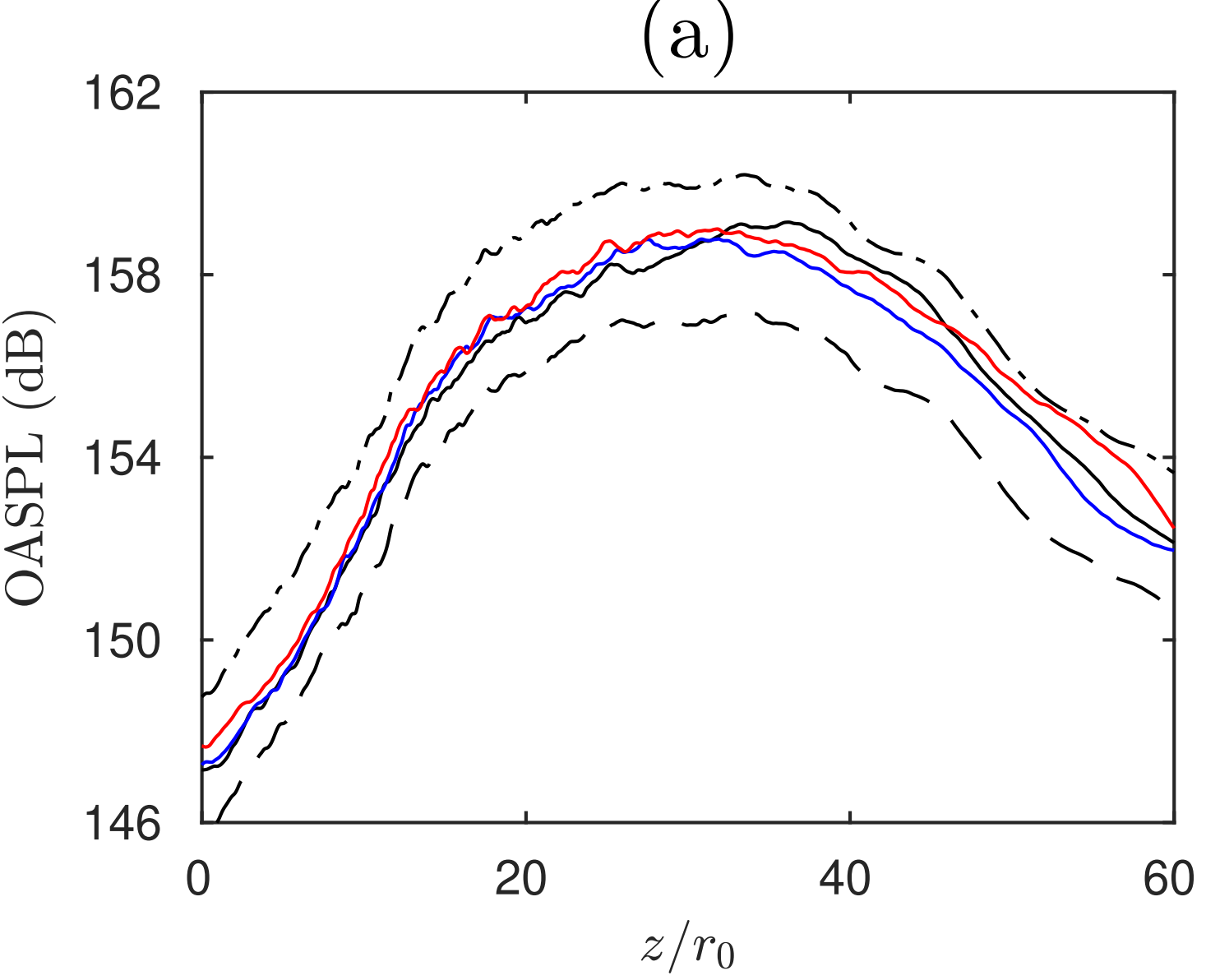
(a)
162
158
154
150
146
OASPL (dB)
0
20
40
60
z/r_0

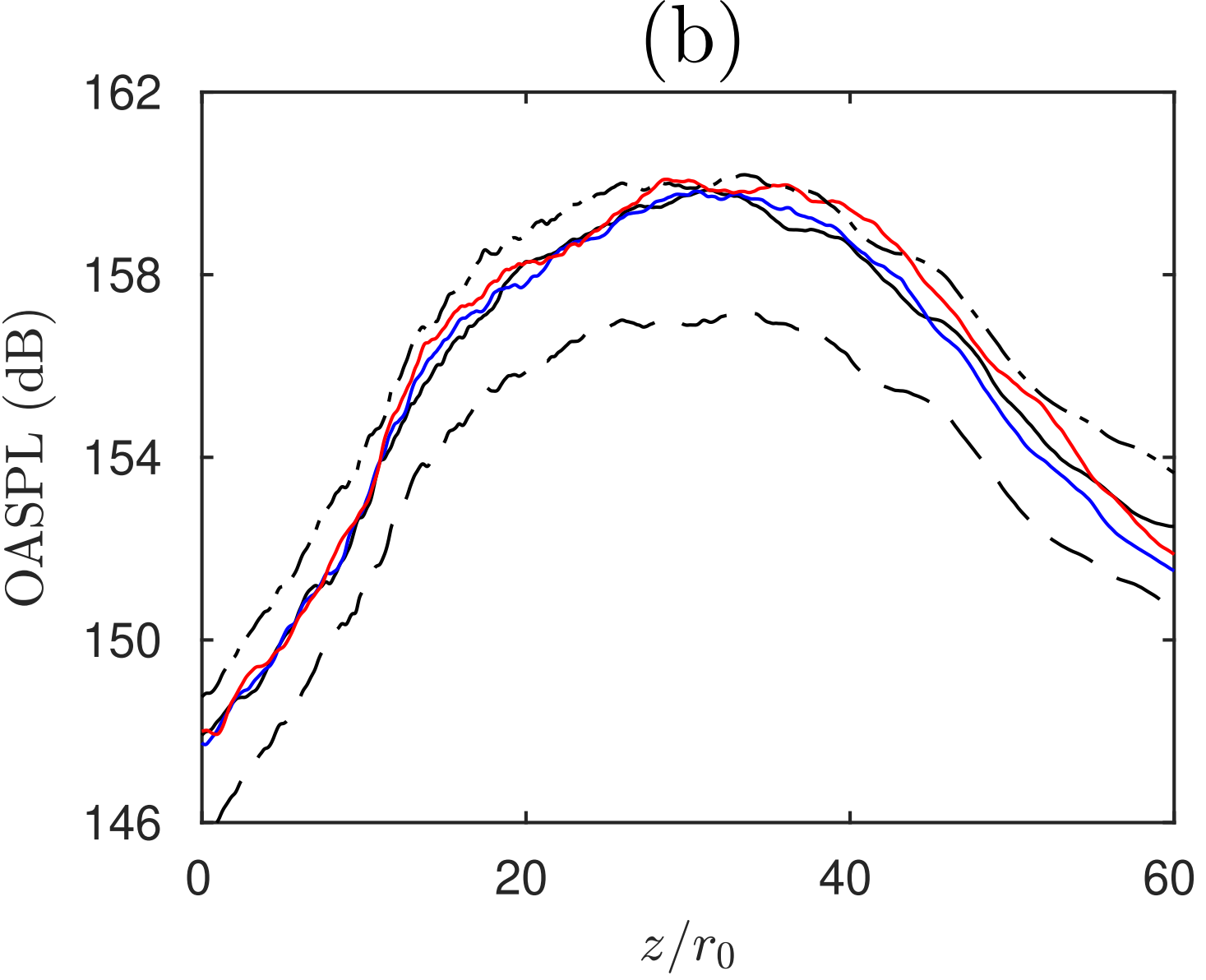
(b)
162
158
154
150
146
OASPL (dB)
0
20
40
60
z/r_0

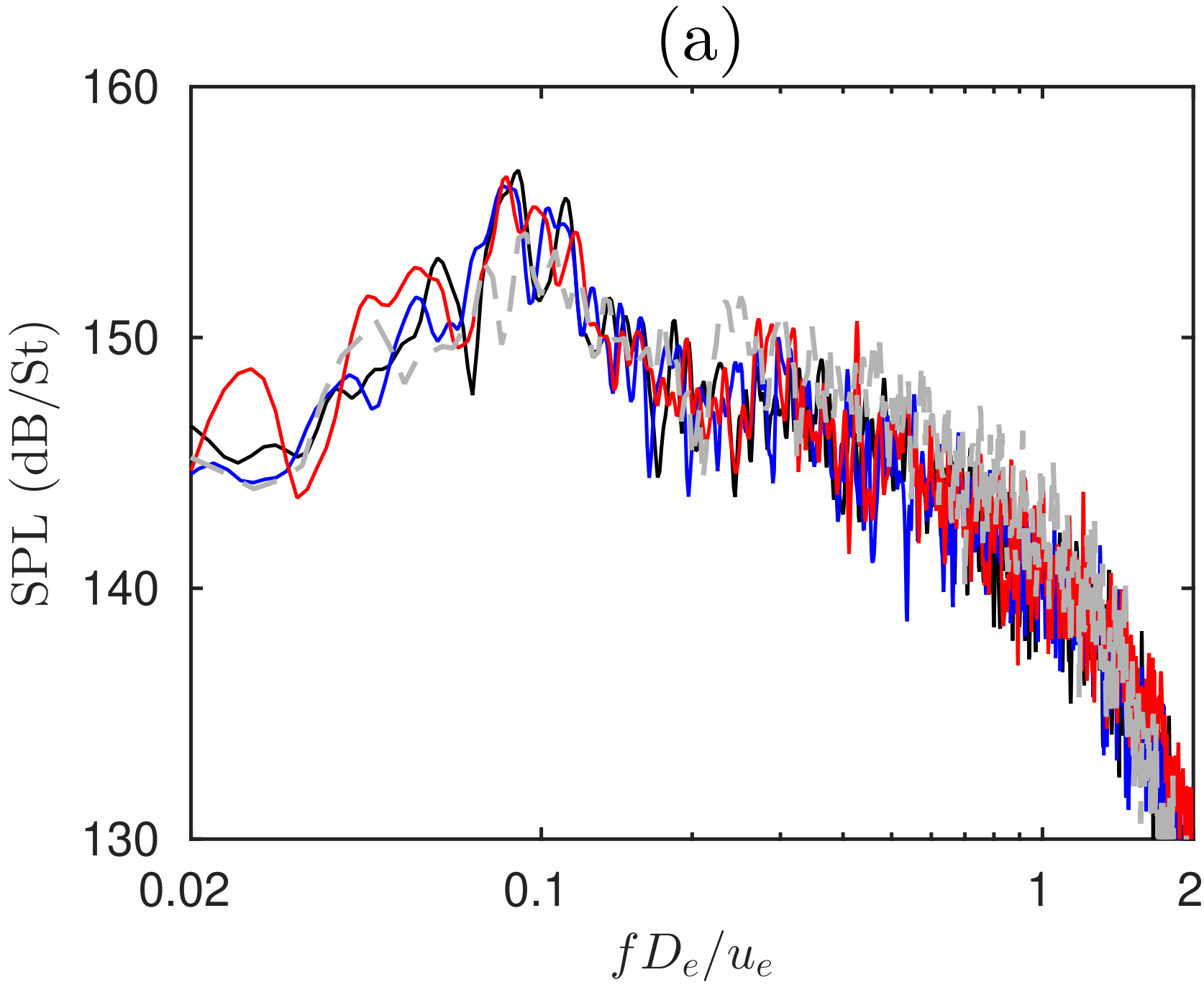
(a)
160
150
140
130
SPL (dB/St)
0.02
0.1
1
2
fD_e/u_e

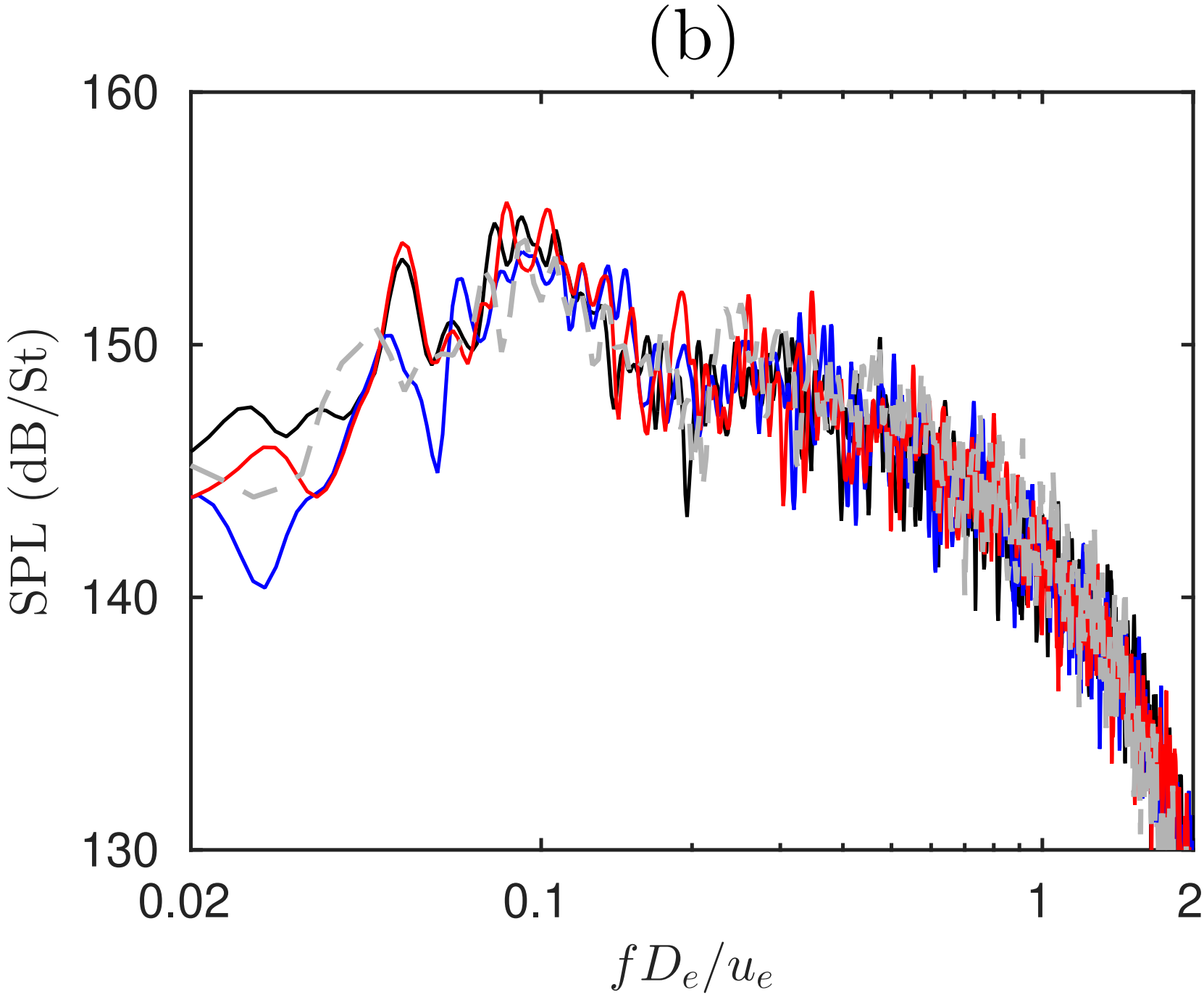
(b)
160
150
140
130
SPL (dB/St)
0.02
0.1
1
2
fD_e/u_e

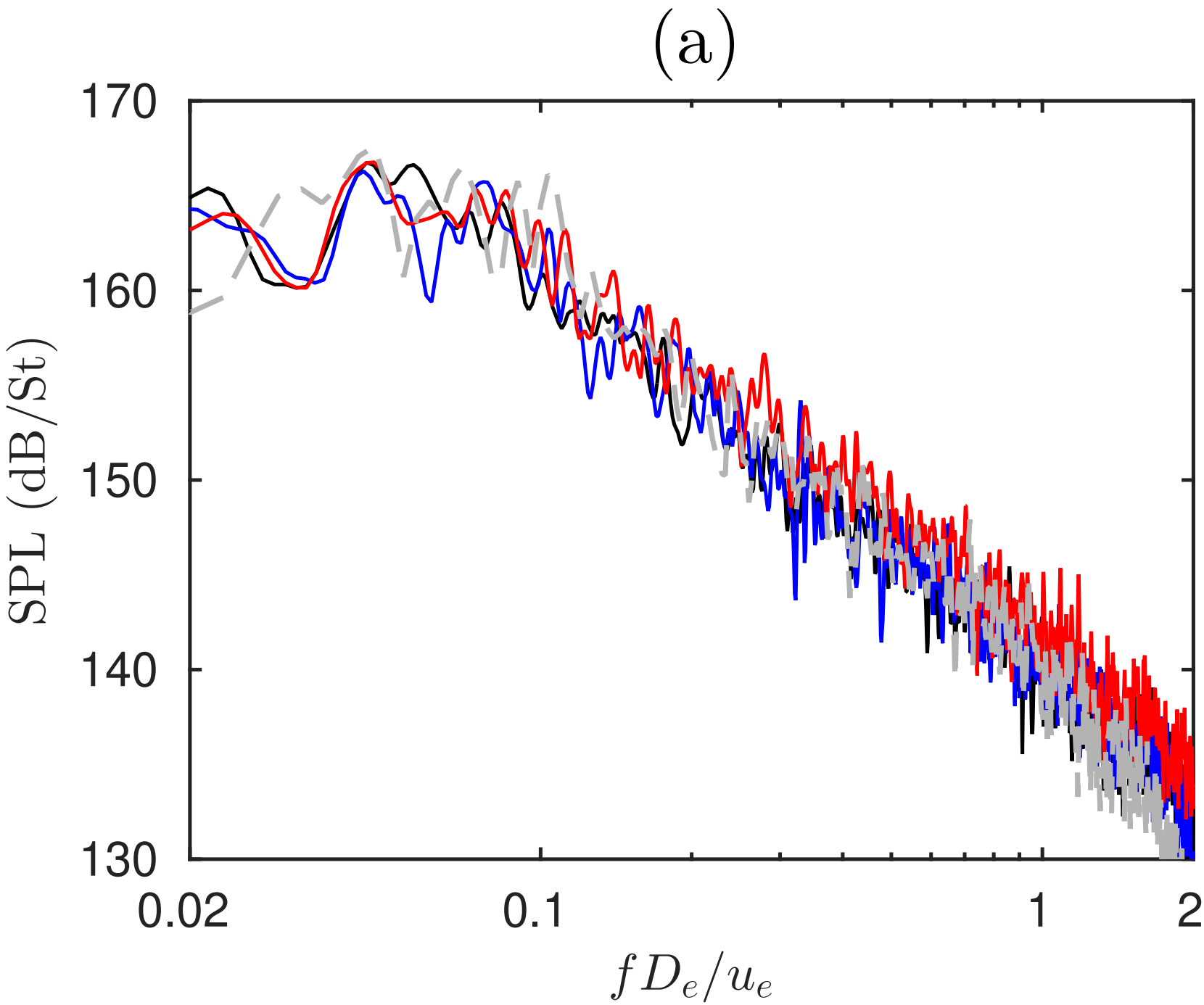
(a)
170
160
150
140
130
SPL (dB/St)
0.02
0.1
1
2
fD_e/u_e

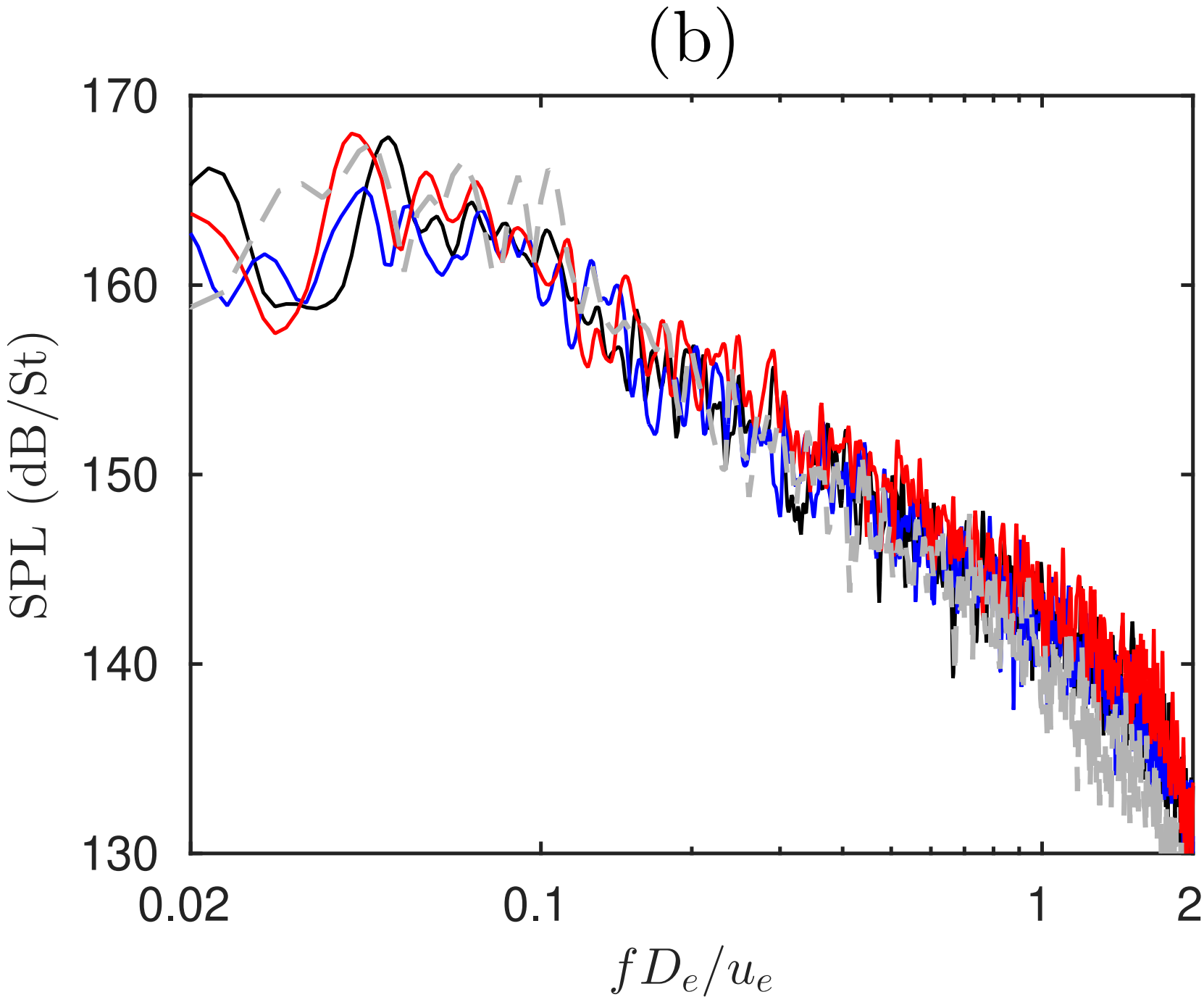
(b)
170
160
150
140
130
SPL (dB/St)
0.02
0.1
1
2
fD_e/u_e

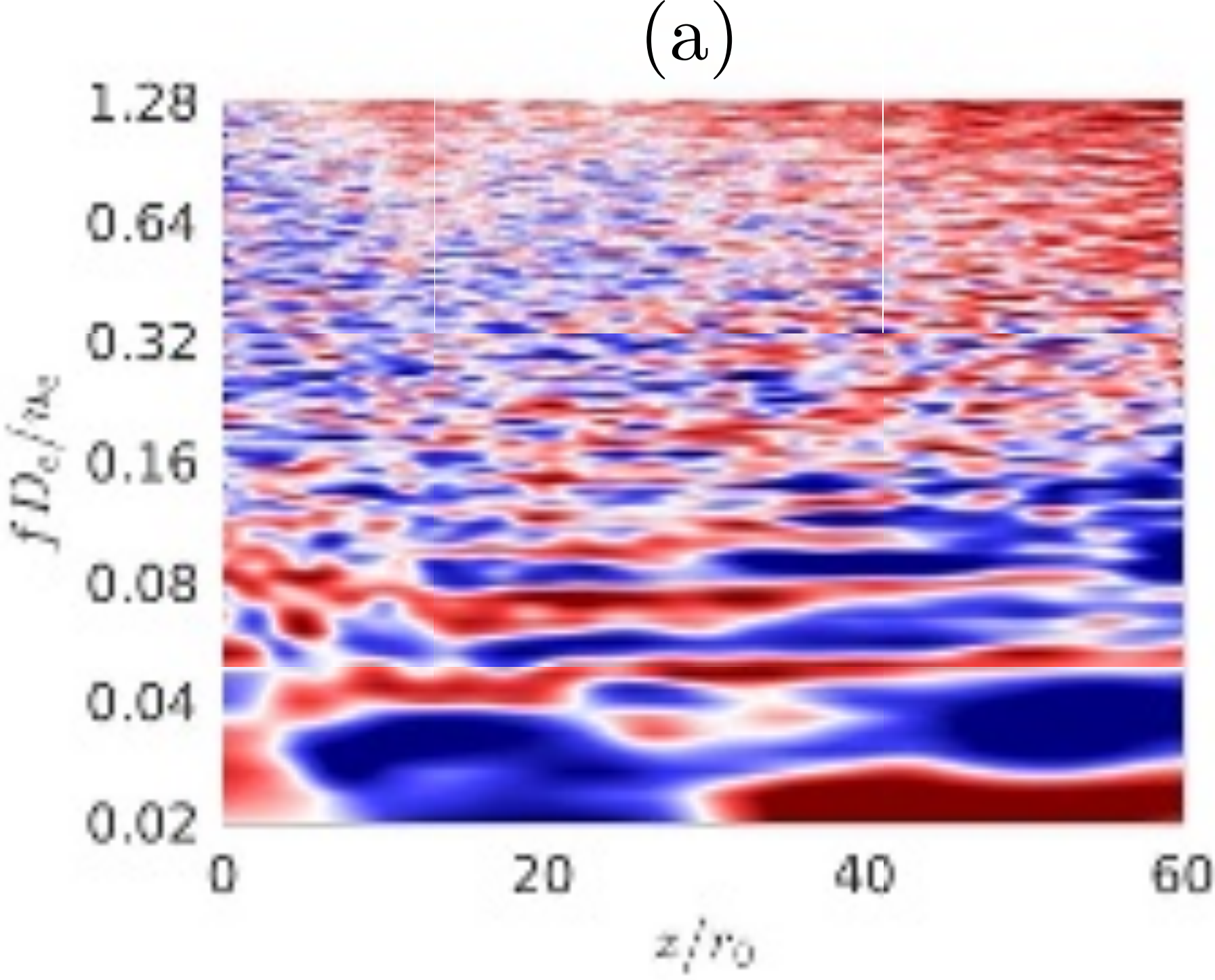
(a)
1.28
0.64
0.32
0.16
0.08
0.04
0.02
fD_e/v_{te}
0
20
40
60
z/r_0

(b)

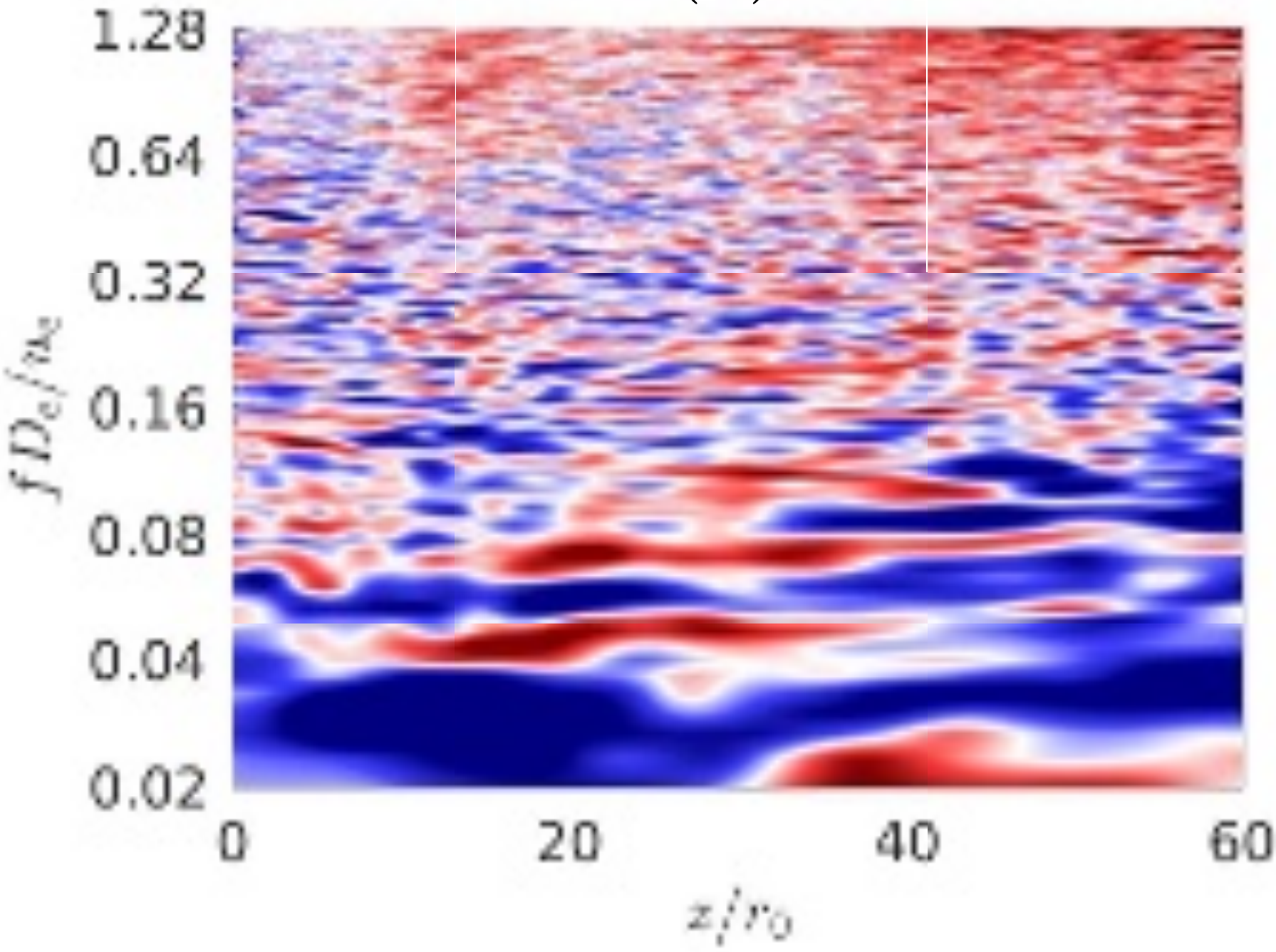

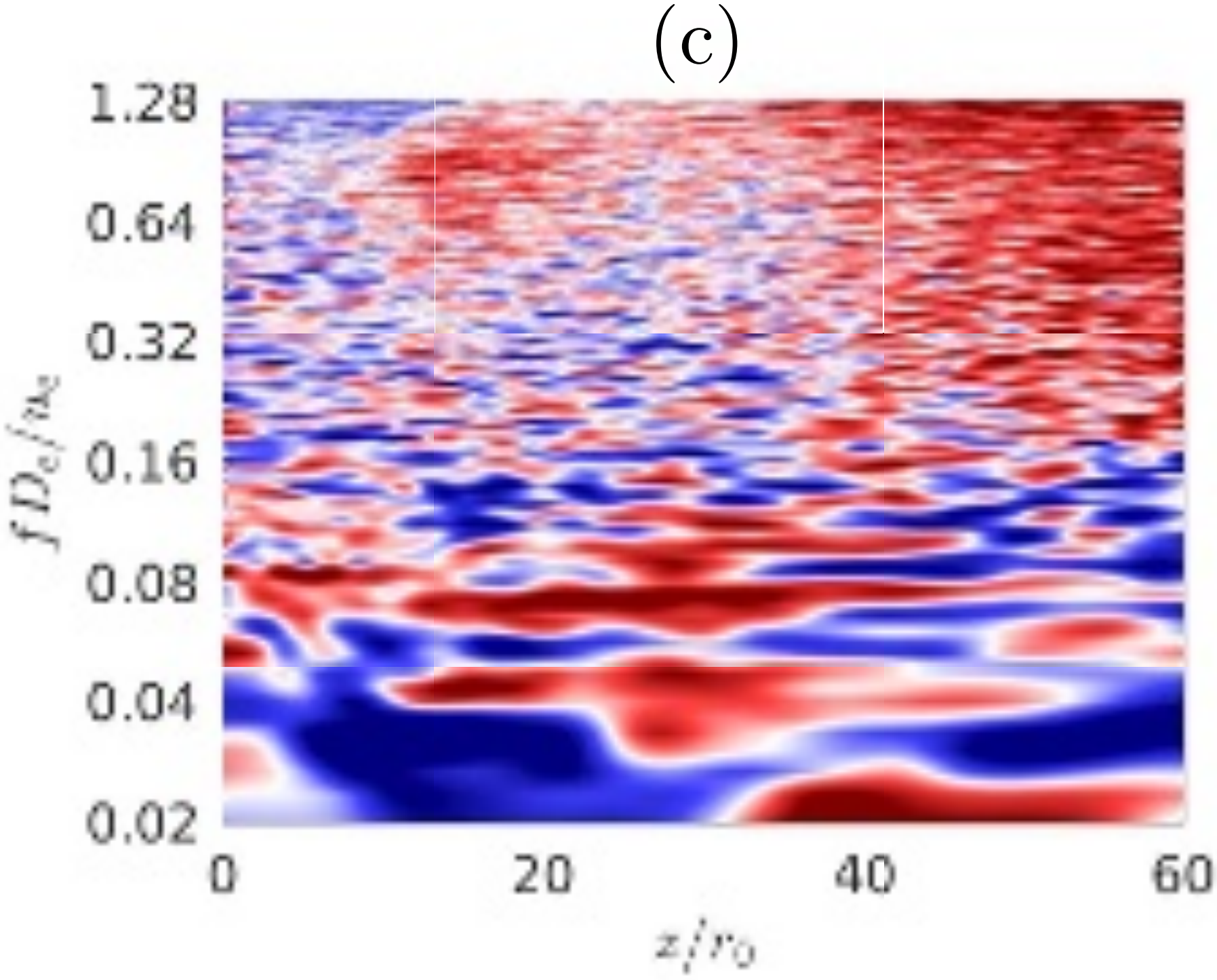
(c)
1.28
0.64
0.32
0.16
0.08
0.04
0.02
fD_e/v_{te}
0
20
40
60
z/r_0